Journal Pre-proofs

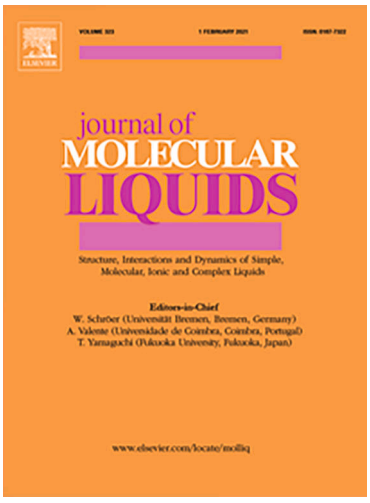

Design and characterization of novel hydrophobic eutectic solvents based on metal-extracting ligands

B. Bernicot, G. Arrachart, S. Dourdain, N. Schaeffer, Gabriel Teixeira, S. Pellet-Rostaing

PII: S0167-7322(25)00499-4
DOI: https://doi.org/10.1016/j.molliq.2025.127332
Reference: MOLLIQ 127332

To appear in: *Journal of Molecular Liquids*

Received Date: 24 October 2024
Revised Date: 3 February 2025
Accepted Date: 6 March 2025

Please cite this article as: B. Bernicot, G. Arrachart, S. Dourdain, N. Schaeffer, G. Teixeira, S. Pellet-Rostaing, Design and characterization of novel hydrophobic eutectic solvents based on metal-extracting ligands, *Journal of Molecular Liquids* (2025), doi: https://doi.org/10.1016/j.molliq.2025.127332

"Design and characterization of novel hydrophobic eutectic solvents based on metal-extracting ligands"

B. Bernicot,[1] G. Arrachart ,[1] S. Dourdain,[1] N. Schaeffer[2], Gabriel Teixeira[2], S. Pellet-Rostaing[1]

[1] ICSM, Univ Montpellier, CEA, CNRS, ENSCM, Marcoule, France

[2] CICECO - Aveiro Institute of Materials, Department of Chemistry, University of Aveiro, 3810-193 Aveiro, Portugal.

Corresponding author: sandrine.dourdain@cea.fr

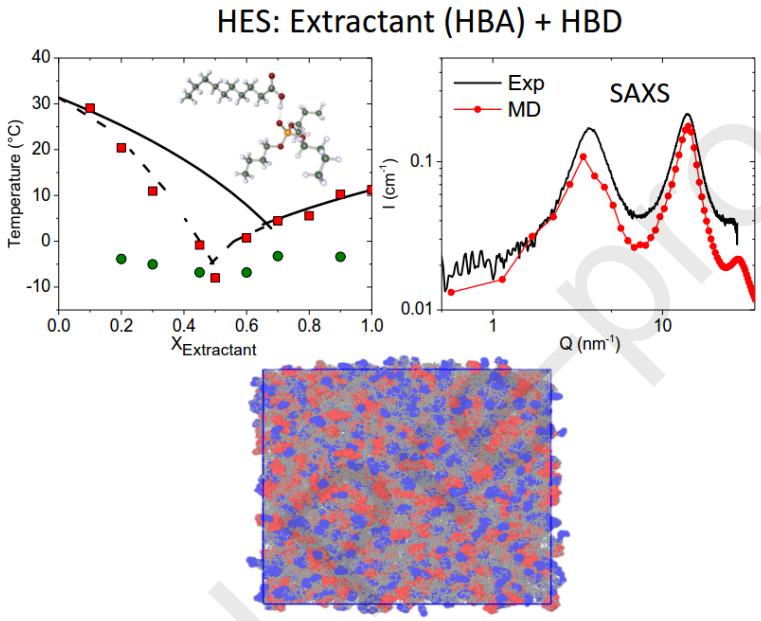

Highlights

Design of new non-ionic Hydrophobic DES using well-known hydrometallurgy extractants as hydrogen bond acceptors and decanoic acid as hydrogen bond donor.

Combined experimental and simulation approaches to investigate the structure and the interactions within these HDES.

Comparison between the experimental phase diagram (DSC) and the ideal phase diagram derived from COSMO-RS model

Interpretation of the HDES structure and eutectic properties thanks to FTIR, SAXS and MD results

Evaluation of physico-chemical properties demonstrating the possible application of these HDES as organic phase for liquid-liquid extraction.

Abstract

In the search for efficient and sustainable liquid-liquid extraction systems, some examples of hydrophobic deep eutectic solvents (HDES) recently emerged as promising alternatives due to their lower volatility, higher stability and extraction performances compared to conventional systems with organic diluents. However, the novelty of HDES has so far limited their study to a small number of systems, precluding further optimization and a deeper understanding. In the present study, we propose the design and full characterization of new non-ionic HDES using a combined experimental and simulation-based approach. These HDES are formulated with extractant molecules that are well known in the field of hydrometallurgy. Specifically, neutral extractants never explored in HDES, such as Tributyl phosphate (TBP), N,N′-dimethyl,N,N′-dioctylhexylethoxymalonamide (DMDOHEMA) or N,N,N′,N′ tetraoctyl diglycolamide (TODGA), were selected as Hydrogen Bond Acceptors (HBA), and associated with decanoic acid (DecA), as a Hydrogen Bond Donor (HBD). A detailed characterization study, using complementary techniques such as FT-IR spectroscopy, small angle X-rays scattering (SAXS) and molecular dynamics (MD), allowed us to elucidate the structural features and intermolecular interactions governing HDES formation. FT-IR and MD revealed quantitatively how the solvent properties are related to hydrogen bond interactions. MD results were successfully exploited to reproduce the experimental SAXS signals, which allowed for the accurate interpretation of the HDES structure. A physicochemical characterization study was further applied to demonstrate the possible application of these HDES as media for liquid-liquid extraction.

Keywords: Hydrophobic eutectic solvents; extraction systems; physicochemical characterization; phase diagrams; molecular and colloidal interactions; H-bond

1. Introduction:

Liquid-liquid extraction is a technique widely used in various fields, particularly well known for its application to the separation of precious metals [1], [2] and rare earth elements [3]. This method involves the juxtaposition of two immiscible phases, namely an aqueous and an organic phase, followed by their phase separation. This process facilitates the transfer of the desired solutes from the aqueous to the organic phase. In metal extraction, this transfer is achieved using extractant molecules possessing a chelating polar head group ensuring metal extraction, as well as a hydrophobic moiety to stabilize the molecule in the organic phase [1], [4]. However, it has important drawbacks, such as the use of significant volumes of effluents that are often environmentally toxic and volatile. These effluents have been associated with air pollution issues such as smog, ozone depletion, and groundwater contamination [1], [2]. In this context, the development of new types of solvents with higher efficiency and a lower environmental impact is crucial [3].

Since the highly cited study of Abbott et al in 2004 [5], deep eutectic solvents (DES) were proposed as substitutes to ionic liquids thanks to their low volatility, high ionicity, and eco-friendliness [6],[7].

The former statement is now seen as a rather broad generalization. Contrary to ionic liquids, DES are binary mixtures such that their properties depend on their component selection. Furthermore, the initial concept of DES, proposed within an electrochemical context that required a conductive media, was expanded to a broader range of mixtures than first conceived. In this study, we will consider that DES

are mixtures of two or more compounds with a melting point deeper than the ideally predicted value, indicating deviation from ideality [8].

The classification of DES mainly encompasses four categories, generally including at least one ionic constituent. The first hydrophobic deep eutectic solvents (HDES) were developed in 2014 by van Osch *et al* [9], [10]. These solvents combined a carboxylic acid as HBD with a long-chain quaternary ammonium as HBA, facilitating the extraction of analytes from aqueous solution by liquid-liquid extraction. Since then, only few examples were studied in depth in the field of metal recovery using DES. The reported studies mainly focus on the use of ionic quaternary ammonium and carboxylic acids for the extraction of metals [11] such as chromium, lithium, iron and platinum group metals [12], [13], [14], [15], [16], [17]. Unfortunately, these ionic HDES suffer from the same drawbacks often directed at ionic liquids, namely their large viscosity and non-negligible cost. Recently, the concept of what constitutes a DES was extend beyond ionic compounds to type V DES, in which mixtures of two non-ionic compounds exhibit strong deviations to ideality stemming from the greater inter-molecular hydrogen bonding relative to that occurring in the pure compounds [8], [18]. Such mixtures, being non-ionic in nature, overcome the traditional issues of ionic DES and increases the potential applicability of HDES. For example, HDES composed of trioctylphosphine oxide (TOPO) [19] as the acceptor combined with bio-derived donors such as fatty alcohol or acids were applied for the extraction of transition and platinum group metals as well as the uranyl cation [4], [20], [21]. Promising results, both in terms of loading capacity and selectivity were observed [8], [11], [13]. However, reported results suggest that the effect of the HDES liquid phase non-ideality and their physicochemical properties on the extraction mechanisms must be considered for their potential application in solvent extraction processes. To exploit the full potential of these high potential solvents for solvent extraction, it is crucial to comprehend the origin of their properties, their structural characteristics and how these properties influence their physicochemical behavior.

In light of the aforementioned problematics, this work focuses on the exploration of new Type V HDES with potential applicability in hydrometallurgical processes, as well as a fundamental structural study to elucidate the dominant liquid phase interactions in these systems. Considering the overarching objective of this work, namely the identification of alternative organic phases for hydrometallurgical separations, various HDES formulations using well-established neutral extractant molecules as HBAs were identified based on their ability to selectively extract specific metal ions. In solvent extraction, the selection of HDES compounds is guided by their ability to facilitate spontaneous separation between the organic and aqueous phases. This requires hydrophobic compounds with low water solubility to minimize HDES loss to the aqueous phase as well as a sufficient density difference from the aqueous phase to ensure efficient and straightforward phase separation. Furthermore, to better appreciate the contribution of the HBA moieties on the resulting HDES properties, extractants spanning a range of coordination mode from mono-, to bi-, and tri-dentate were selected, namely the monodentate tributyl phosphate (TBP) [16], [17] and TOPO [13], [18], the bidentate *N*,*N*′-Dimethyl,*N*,*N*′-dioctylhexylethoxymalonamide (DMDOHEMA)[25], [26], [27], and the tridentate *N*,*N*,*N*’,*N*’ Tetraoctyl Diglycolamide (TODGA) [22], [23]. To facilitate the interpretation of the results, a common HBD was used across all systems: decanoic acid (DecA). DecA is one of the most commonly used HBD in HDES synthesis. As a fatty acid with a long hydrophobic alkyl chain, it significantly enhances the overall hydrophobicity of the eutectic solvent. Additionally, DecA is biocompatible and has low toxicity, making it an environmentally friendly option for various applications [30]. Although DecA can be considered as an “imperfect” HBD due to the well-known stability of the carboxylic dimer, it is resistant to oxidative degradation, unlike phenolic compounds (such as thymol), an important criterion for the application of such systems in the separation of metals (more precisely lanthanides elements) from nitric acid solutions. The chemical structures of all components are shown in **Figure 1**, highlighting the groups that act as potential acceptor and donor sites. The solid-liquid equilibrium (SLE) phase diagrams were measured by differential scanning calorimetry (DSC), with COSMO-RS shown to correctly estimate the latter. Further information on the molecular and colloidal interactions between the various HBA and HBD was gathered by Fourier transform infrared spectroscopy (FT-IR) and small-angle X-ray scattering (SAXS), both corroborated by molecular dynamics (MD) simulations. The findings disclosed not only

novel HDES for potential hydrometallurgical applications, but also shed light on the interactions driving Type V DES formation, facilitating the future identification of potential mixtures.

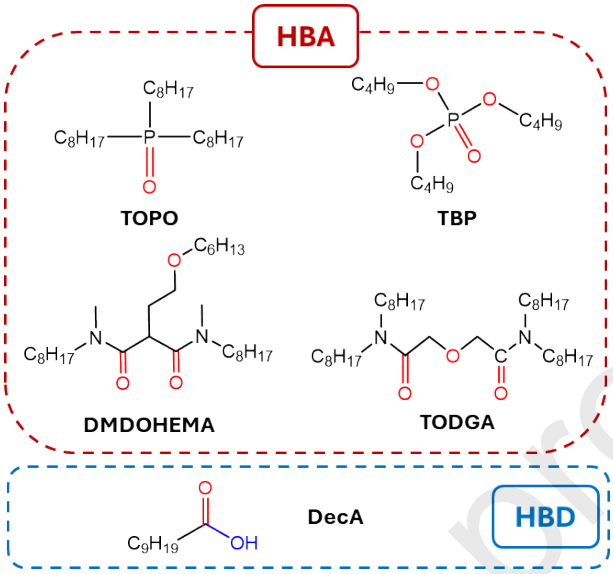

Figure 1: Structure and acronyms of the hydrogen bond acceptors (HBA) and donors (HBD) molecules used in this work, with the potential acceptor and donor sites highlighted in red and blue respectively.

2. Materials and methods

a) Chemicals

All chemicals reagents including decanoic acid (DecA, 99% purity), trioctylphosphine oxide (TOPO, 99% purity) and tributyl phosphate (TBP, 99% purity) were purchased from Sigma-Aldrich (France), *N*,*N*′-Dimethyl,*N*,*N*′-dioctylhexylethoxymalonamide (DMDOHEMA, 99% purity) was purchased from Creative Chemistry (UK). The chemicals were used as received from the supplier without further purification. *N*,*N* ,*N*',*N*' Tetraoctyl Diglycolamide (TODGA, 98% purity) was synthesized according to a procedure adapted from the literature with the ^{1}H NMR (**Figure S1**) characterization in agreement with those referenced [31], confirming its purity.

b) HDES preparation, determination of phase diagrams and SLE modeling

The binary mixtures of extractant (HBA) with decanoic acid were prepared gravimetrically in glass vials in different proportions covering the full composition range (at 0.1 mole fraction intervals). After mixing by magnetic stirring (300 rpm) and heating at 60°C until a homogeneous liquid was obtained, the mixtures were left to cool at room temperature for 8 hours prior to use. All HDES were prepared under ambient conditions and atmosphere. Differential Scanning Calorimetry (DSC) was used to determine the phase diagram of the different mixtures: TBP:DecA, TODGA:DecA and DMDOHEMA:DecA. The measurements were conducted under atmospheric pressure coupled to an electric cooling unit in University of Aveiro, Portugal where the measurements were made using, DSC 7000X® from Hitachi A mixture sample (between 5 and 25 mg) was transferred to an aluminum crucible and sealed using a PerkinElmer AD6 micro-analytical balance with an accuracy of ± 0.006 mg. First, the samples were cooled to −100°C at 5°C min^{-1}. After a 5 minutes isotherm, a heating rate of 4°C min^{-1} was applied to reach 150°C. The melting temperature is taken at the maximum melting peak.

Neglecting heat capacity effects, the SLE of the eutectic mixtures with complete immiscibility in the solid phase can be described by equation (1) [32], [33]:

$$\ln\left(x_i\gamma_i^l\right) = \frac{\Delta_m H_i}{R}\left(\frac{1}{T_{m,i}} - \frac{1}{T}\right) \quad (1)$$

where x_i is the mole fraction of component i and γ_i^l its activity coefficient in the liquid phase, T is the absolute temperature, R is the ideal gas constant, $T_{m,i}$ and $\Delta_m H_i$ are the melting temperature and enthalpy of the pure solute, respectively. When the differences between the eutectic and the melting temperatures of the pure compounds are small (< 100 K), as is the case in the studied systems, the term related with heat capacities may be neglected due to its small contribution to the phase equilibrium calculations. For those systems where the eutectic temperature differs by less than 100 K from the melting temperature of decanoic acid (31.35°C), the heat capacity must be considered in equation (1). This changes equation (1) to equation (2). As the heat capacity of pure decanoic acid in liquid phase is unknown, the heat capacity of pure nonanoic acid in the liquid phase (327.28 J/K.mol) [34] has been used for these cases.

$$\ln\left(x_i\gamma_i^l\right) = \frac{\Delta_m H_i}{R}\left(\frac{1}{T_{m,i}} - \frac{1}{T}\right) - \frac{\Delta_m Cp_i}{R}\left(1 - \frac{T_{m,i}}{T} + \ln\left(\frac{T_{m,i}}{T}\right)\right) \quad (2)$$

Where $\Delta_m Cp_i$ is the difference of the molar Heat capacity in the liquid phase and in the solid phase of the component i at the melting point temperature.

When ideality is assumed, γ_i equals to 1 and the solubility curves are derived from Equation (1). The experimental activity coefficients are obtained through Equation (1) using the experimental temperature data.

c) Investigation of HDES hydrogen bonding

Fourier Transform Infrared Spectroscopy (FTIR) was carried out between 615 to 4000 cm^{-1} on a Perkin Elmer (Wellesley, MA, USA) Spectrum 100 spectrometer with an Attenuated Total Reflectance (ATR) transmission mode with resolution of 4 cm^{-1}. Each measurement was repeated four times. The HDES samples were added directly to the spectrometer in a volume of 50 µL as a function of the composition at ambient temperature.

For the deconvolution the Origin 2015 (Acamedic version) software was used. The baseline was subtracted using interpolations and the peaks were fitted using a Gaussian function to determine the area, maximum intensity, and full-width at half maximum.

d) Structural analysis of the HDES liquid phase

Small Angle X-rays Scattering (SAXS) measurements were carried out on a home-built instrument at the ICSM (Marcoule, France) using a bench built by Xenocs with a molybdenum anode as X-ray source (0.71 Å) and a MAR Research 345 detector at 770 mm from the sample. Calibration was performed using a polyethylene standard with data treatment using PySAXS 3.26 and all the samples were measured in quartz capillary of 2 mm of thickness with a sample volume of 70 mL.

e) Determination of physico-chemicals properties

The viscosity measurement was performed with a Microvisc from Rheosense at 25°C with a shear rate of 200 s^{-1}, two microchips were used one for a viscosity range from 0 to 100 mPa.s and the other with a

range from 60 to 5000 mPa.s. Reported values are the average of 5 measurements with an error of less than 5%. The samples are added in the microviscosimeter using a pipette and a volume of 100 µL. The microviscosimeter uses VROC® microfluidic technology, this sensor measures viscosity from the pressure drop of a liquid as it flows through a rectangular slit.

The density measurements were performed with a DSA 5000 thermoregulated digital densimeter (Anton Paar). The apparatus measures densities using an oscillating U-tube with an accuracy of 0.00001 g/cm3 and temperature controlled to within 0.001 °C. All measurements were conducted at 25.005 ± 0.004 °C The samples are added directly into the densimeter with a syringe in a volume of 1 mL.

For the viscosity and density measurements, the HDES were used after their preparation to ensure that no recrystallization occurs.

The solubility of the HDES in the aqueous phase was determined by measuring the concentrations of the organic compounds in the aqueous solutions after the contact of the HDES with water (1:1 v/v) by determining the total organic content (TOC) using a Shimadzu TOC-VCSH analyzer based on a 680 °C combustion catalytic oxidation/NDIR method. The loss of organic phase in the aqueous phase wasmeasured after the two phases were contacted for 1 h at 250 rpm in a thermostatically controlled cell (Infor-ht® ecotron) at 25 ◦C and centrifuged at 8000 rpm and 25°C for 10 minutes (Rotina 380R).To measure the water content in the organic phase and the organic content in the aqueous phase after contact with water, the two phases were contacted for 1 h at 250 rpm in a thermostatically controlled cell (Infor-ht® ecotron) at 25 ◦C and centrifuged at 8000 rpm and 25°C for 10 minutes (Rotina 380R).The water content in the HDES phase following extraction was determined using a volumetric Karl-Fischer titrator (Metrohm 809 titrando) with an Hydranal® solution from Sigma-Aldrich.

f) COSMO-RS simulations

COSMO-RS is a thermodynamics model [35], [36] that was used to predict the solid-liquid equilibrium of the different neutral extractant + DecA systems and also their activity coefficients. To use this model the molecules were first optimized by DFT using the COSMO-BP-TZVP-fine template available in the TmoleX software. This template adopts a def-TZVP_fine basis set for all atoms with the B-P86 functional and the COSMO solvation model (continuum with infinite permittivity). The molecule files obtained were used as input for the COSMOtherm software using the BP_TZVP_fine_21 parametrization. The charge density is calculated by the COSMO-based model, placing the molecule into a cavity within a conducting medium. This process solvates the molecule, resulting in surface screening around it. This screening translates into a surface charge distribution, leading to the formation of a sigma profile. The generated sigma profiles provide information on the charge density (represented as sigma σ) of the molecules being investigated, which the model uses to compute activity coefficients.

g) Molecular Dynamic simulations

Molecular dynamics (MD) simulations were carried out using Gromacs 2023 package [37] within the NpT ensemble by adopting the leapfrog algorithm to integrate the equations of motion at a fixed temperature (298 K) and pressure (1 bar) [38]. The OPLS all-atom force field [39] was used for all molecules, the topologies for all extractants were generated using LigParGen [40], [41]. The Lennard-Jones (LJ) potential and the Coulomb term were considered for non-bonded interactions. Hydrogen bonds were constrained by the LINCS algorithm [42] whilst LJ and Coulombic interactions were computed up to a cut-off radius of 1.2 nm. The force-switch van der Waals potential modifier was employed for LJ, where the energy decays smoothly to zero between 0.9–1.2 nm. All simulations were started from a randomly distributed configuration, and production runs were carried for 40 ns with a time step of 2 fs following an energy minimization step using the steepest descent algorithm and two short equilibrium runs in the NVT and NpT ensembles, respectively. The temperature and pressure were controlled through the Nose–Hoover thermostat [43] and the Parrinello–Rahman barostat [44], respectively. All analysis was carried out on the last 20 ns of the simulation run. MD simulation outputs

were visualized using the VMD [45] software package. SAXS profile, radial distribution functions (RDFs) and coordination numbers (CNs) were calculated using Gromacs inbuilt analysis tools. Spatial Distribution Functions (SDFs) and Domain Analysis via Voronoi Tesselation were performed using the TRAVIS post-processing package[46], [47].

For clarity, a schematic illustration is provided in ESI to outline the various experiments conducted in this article (**Figure S2).**

3. Results and Discussion

a) Phase diagram

Hydrophobic deep eutectic solvents, referred to as eutectic systems, exhibit a decrease in the melting point of the mixture compared to the melting temperatures of pure compounds. This phenomenon is primarily attributed to a negative deviation from ideality due to favorable intermolecular interactions between the donor and the acceptor, specifically in the form of hydrogen bonds (not only), which facilitates the reduction of the melting point. A proven approach to the preparation of Type V DESs presenting negative deviations from ideality when mixed with common HBDs is through the inclusion of HBAs [18] that do not possess HBD sites. Due to their inability to self-interact through hydrogen bonding, such lone HBAs readily form hydrogen bonded aggregates upon inclusion of HBDs, resulting a more pronounced decrease in the melting point. The SLE phase diagrams for the lone HBAs TOPO, TBP, DMODHEMA, and TODGA with DecA were measured by DSC and are shown in **Figure 2** along with the ideal SLE calculated from equation (1) and the COSMO-predicted SLE for each system. The experimental SLE data is reported in **Tables S1,** along with the activity coefficients estimated from equation (1), whilst the melting properties of the pure compounds are presented in **Table 1**.

Table 1: Experimentally measured melting temperature (K) and enthalpy (kJ/mol) for the different compounds used.

Compounds	**Abbreviation**	**M_w (g/moL)**	**T_m (K)**	**ΔH_m (kJ/mol)**	**Cp (at 300K in J/K.mol)**
Decanoic acid[a]	DecA	172.26	303.8	27.82	541.18[d]
Trioctylphosphine oxide[b]	TOPO	386.65	325.9	58.02	/
Tributylphosphate[c]	TBP	266.32	194.15	/	/
N,*N*′-Dimethyl,*N*,*N*′-dioctylhexylethoxymalonamide[c]	DMDOHEMA	482.78	284.2	36.87	/
N,*N* ,*N*',*N*' Tetraoctyl Diglycolamide[c]	TODGA	582	284.39	36.90	/

[a] Taken from [48]; [b] taken from [21]; [c] this work; [d] Taken from [34]

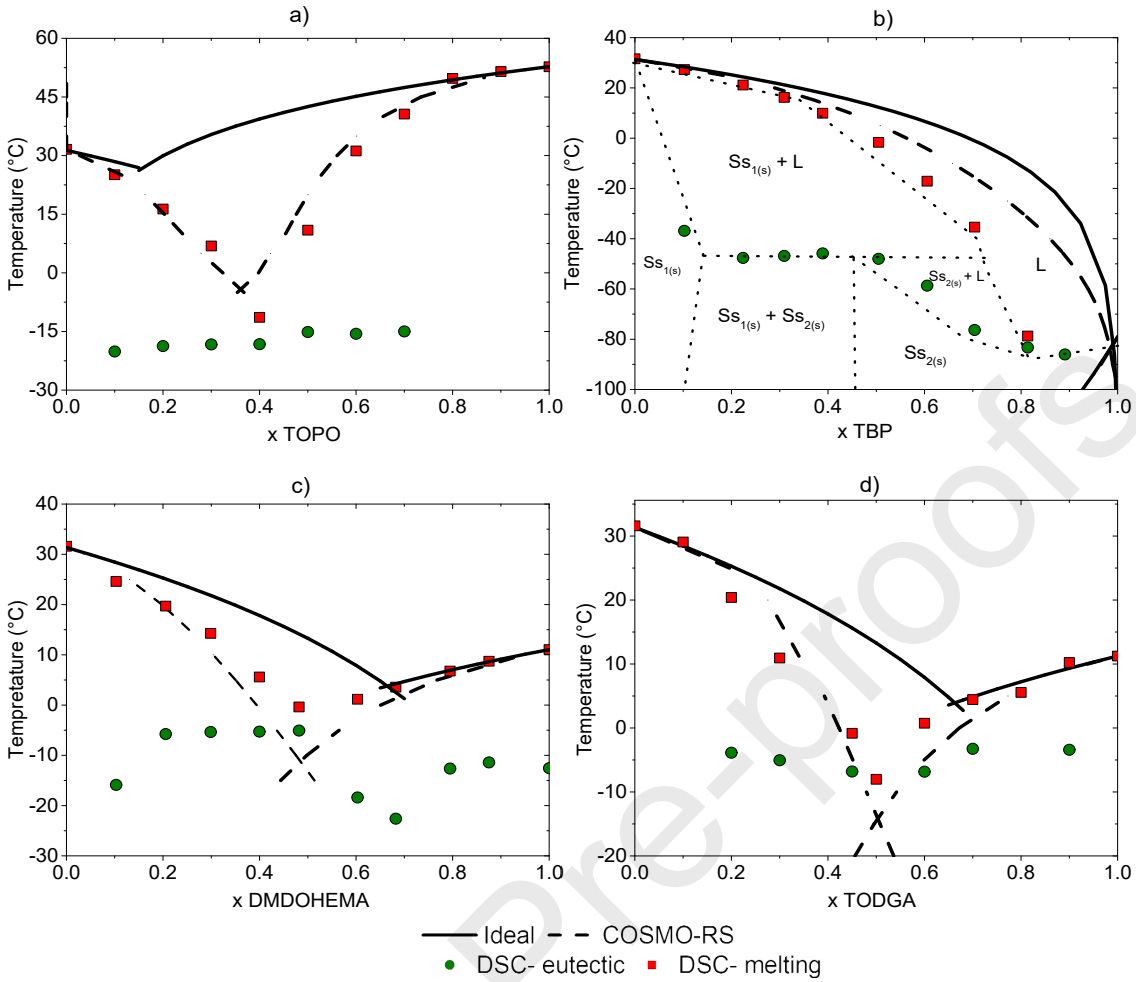

Figure 2: Phase diagram of (a) TOPO + Decanoic acid adapted from *[21]* (b) TBP + Decanoic acid (c) DMDOHEMA + Decanoic acid and (d) TODGA + Decanoic acid

The COSMO-RS sigma profile and surface for each of the five studied components are available in **Table S2** and **Figure S3 to S7** of the Support Information, and provide information about the molecular interactions of the different components of the HDES [49]. The SLE diagram of the TOPO:DecA system was previously reported and was not determined as part of this work but was included for comparative purposes [21]. Due to problems in the crystallization of TBP at some compositions, no phase transitions could be measured. Except for the case of TBP in which only a qualitative description of the SLE was obtained, COSMO-RS was able to correctly predict and reproduce the experimentally obtained phase diagrams for the TOPO, DMODHEMA, and TODGA systems with DecA.

Such findings add to the existing literature and confirm the suitability of COSMO-RS as a computationally efficient approach for the screening and modelling of existing and new Type V eutectic mixtures. Although the pure HBAs are liquid close to ambient temperature and could therefore be directly used as solvents (as is sometimes the case for TBP [50], [51]), the purpose of this study is to better appreciate how the inclusion of molecules containing such functions influences the deviations to ideality, and to provide guidelines to design systems with other HBAs for future applications.

All mixtures exhibit a phase behavior characterized by a single eutectic point with a wide operational liquidus range under ambient temperatures, and present notable deviations to ideality as demonstrated by the activity coefficients in **Table S1**. The phase diagram of TOPO:DecA mixtures is presented in **Figure 2a**. For x_{TOPO}= 0.4, the melting point is depressed of 38.9 °C below the predicted value for an ideal system. This mixture allows the formation of liquids at room temperature in the composition range x_{TOPO}= 0.20–0.55. Similarly, the phase diagram of the bidentate DMODHEMA and tridendate TODGA

extractants with DecA in **Figure 2c** and **2d** respectively, exhibit a similar phase behavior characterized by a single eutectic point at x_{DecA}= 0.5. The eutectic temperature of -5°C differs from the ideal phase diagram, which estimates that the eutectic occurs at extractant ratios of $x_{DMDOHEMA}$ and x_{TODGA} = 0.7, with a corresponding temperature of around +5°C. At 20°C for the TODGA and DMOHEMA systems, the usable compositions are between xDecA = 0.75 to xDecA = 0. The similar behavior for both systems may be due to the presence of identical amide functional groups in their structure. Interestingly, the presence of ether moieties at different locations in each molecule, namely the alkyl tail for DMDOHEMA and the polar head for TODGA, does not appear to greatly influence the resulting phase behavior, or indeed the melting properties of each individual compounds (see **Table 1**), despite the potentially greater configurational entropy of the TODGA the polar head group. This suggests that potential steric hindrances to the HBA-HBD interactions are at play, limiting the stoichiometry of possible intermolecular associations. The absence of significant difference between the HBA for these two systems is further reflected in the similarity of their COSMO sigma profile in **Figure S5** and **S6**, confirming their comparable HBA capacity, translating in similar phase behavior.

The analysis of the TBP system in **Figure 2b** is more complex than that of the other systems. First, the limited range of melting point measurements arises from TBP's melting temperature of -79°C, which is close to the DSC's minimal measuring capability of -80°C. Only deviations from ideality were noted in the decanoic acid segment. Second, the observation of different transitions suggests some solid behaviors at low temperature for some compositions. As these possible solid transitions where not taken into account during the COSMO-RS representation of the SLE, a poor quantitative description was obtained similarly to that reported for other systems with such solid behavior, showing some limitations of the model when applied to more complex systems [49].

Contrary to the TOPO system in which strong deviations to ideality are observed on the TOPO-rich side of the SLE, for the TODGA and DMDOHEMA systems significant deviations from ideality occur on the HBD side, similarly to that observed for TBP. This discrepancy may be due to the difference in physical state between TOPO, with a melting temperature of 52.8 °C, and the other extractant being liquid at room temperature. Furthermore, molecules such as TODGA were reported to present limited self-association in their pure state through dispersive interactions (head-head contact)[52]. In an attempt to provide a more objective comparison of the different systems, the activity coefficient of each component at the eutectic composition as well as the standardized metric proposed by van den Bruinhorst et al [53] for the assessment of a eutectic system's "deepness" (D_e), calculated as per equation 2, are summarized in **Table 2**.

$$D_e = 100 * \frac{T_e - T_e^{id}}{T_e^{id}} \quad (2)$$

T_e and T_e^{id} are the experimental and ideal temperature at the eutectic composition respectively. Unfortunately as the eutectic composition could not be estimated for TBP:DecA system, no such comparison could be made. The presence of electron withdrawing group and delocalization of the partial charge across the polar head results in a change of the basicity of the various extractant, proceeding from more to less basic as follows TOPO > TBP > DMODHEMA ≈ TODGA. This trend matches well that provided by the COSMO-RS sigma profiles, which predict a greater HBA character for TOPO, followed by TBP, DMODHEMA, and TODGA (**Figures S3 to S6**). These tendencies are in accordance with those for the obtained D_e and $\gamma_{e,I}$ values in **Table 2**, suggesting that augmenting the basicity difference between the hydrogen bond donor and acceptor, in the absence of proton transfer, correspondingly increases the non-ideality of the system and its "deep" character. Relating these findings to classical solvent extraction systems, although mixed extractants are commonly used for synergistic extraction, their self-interactions are often neglected despite their complex extraction tendencies [54]. These interactions, which causes deviation to ideality, clearly show that processes with neutral and acidic extractant need to be investigated with adequate simulation.

Table 2: Eutectic composition, experimental eutectic temperature (T_e), ideal eutectic temperature (T_e^{id}) calculated from equation (1), their difference ΔT_e, the eutectic depth De of the differents mixtures as defined in (2), and the experimental activity coefficient ($\gamma_{e,i}$) of component *i* at near the eutectic composition.

HBA	Eutectic composition (x_{DecA})	T_e (°C)	T_e^{id} (°C)	ΔT_e (°C)	D_e	$\gamma_{e,HBA}$	$\gamma_{e,HBD}$
TOPO	0.6	-12.15	26.85	39.0	-13.0	0.01	0.28
DMDOHEMA	0.5	-11.15	4.25	15.4	-5.6	1.04	0.557
TODGA	0.5	-8.15	4.85	13.0	-5.0	0.64	0.46

The interpretations drawn from the activity coefficients of these systems are analogous to the D_e analysis. As can be observed in Figure 3, the deviations from ideality of decanoic acid in TBP, DMODHEMA, and TODGA mixtures are similarly negative. Meanwhile, the deviations of DMODHEMA and TODGA in decanoic acid mixtures are near-ideal. On the other hand, both the deviations of decanoic acid and TOPO are much lower than in the mixture of the other three compounds. It is interesting that TOPO and TBP behave differently though they both have a similar HBA site. Although their difference in basicity may explain their distinct behaviour, the discrepancy of their apolar region must also be taken into account and may help to justify the greater cross interactions of TOPO with decanoic acid. However, it is worth noting that the impressively negative deviations shown in the TOPO eutectic mixture can hinder its potential as a metal extracting medium, since it may imply that the P=O sites are not available for metal binding. This aspect will be further discussed later.

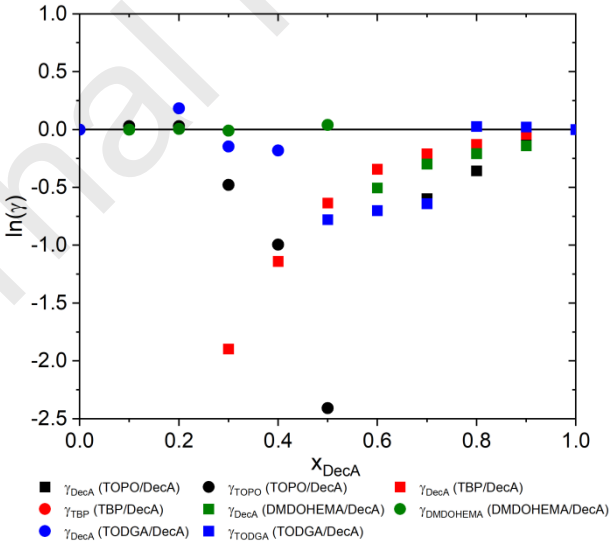

Figure 3: Non-isothermal activity coefficients of Decanoic acid with TOPO (black symbols) adapted from *[21]*, TBP (red symbols), DMDOHEMA (green symbols), TODGA (blue symbols). Symbols represent the activity coefficient of decanoid acid (squares) and the second compound (circle).

b) Hydrogen-bond analysis of the liquid phase

Having characterized the SLE phase diagrams, attention is now paid to the understanding of the liquid phase structure by FTIR and its organization by SAXS and classical MD. The change in the dominant hydrogen bond interactions upon mixing, which was previously identified as the locus of the "deep" eutectic behavior, was followed by infrared spectroscopy [8]. The obtained spectra for each HDES for various compositions at 0.1 mole fraction intervals within the liquidus window at 20°C are presented in **Figure 4**. To ensure that all comparisons are performed between samples in the liquid state, octanoic acid was used for reference for the x_{HBD}=1.0 composition, as pure decanoic acid is solid at 20°C. The bands classically assigned to such hydrogen bonds were examined with a particular focus on the stretching vibration of the P=O bond between 1250 and 1300 cm^{-1} for the TOPO and TBP extractants [55]. For the TODGA and DMDOHEMA extractants, the analysis focused on the carbonyl C=O stretching vibrational frequency ($\nu_{C=O}$) located at 1650 cm^{-1}[56]. The band at 1050 cm^{-1} that can be assigned to the C-O-C stretching vibration of DMDOHEMA and TODGA was also examined [57], [58]. The carbonyl stretching vibration maximum ($\nu_{C=O}$) at 1710 cm^{-1} of pure fatty acids was previously assigned to the carboxylic dimer, with the appearance of upshifted wavenumbers at 1740 cm^{-1} assigned to the weakening of the dimer upon HBA inclusion and the formation of intermolecular hydrogen bond aggregates[59].

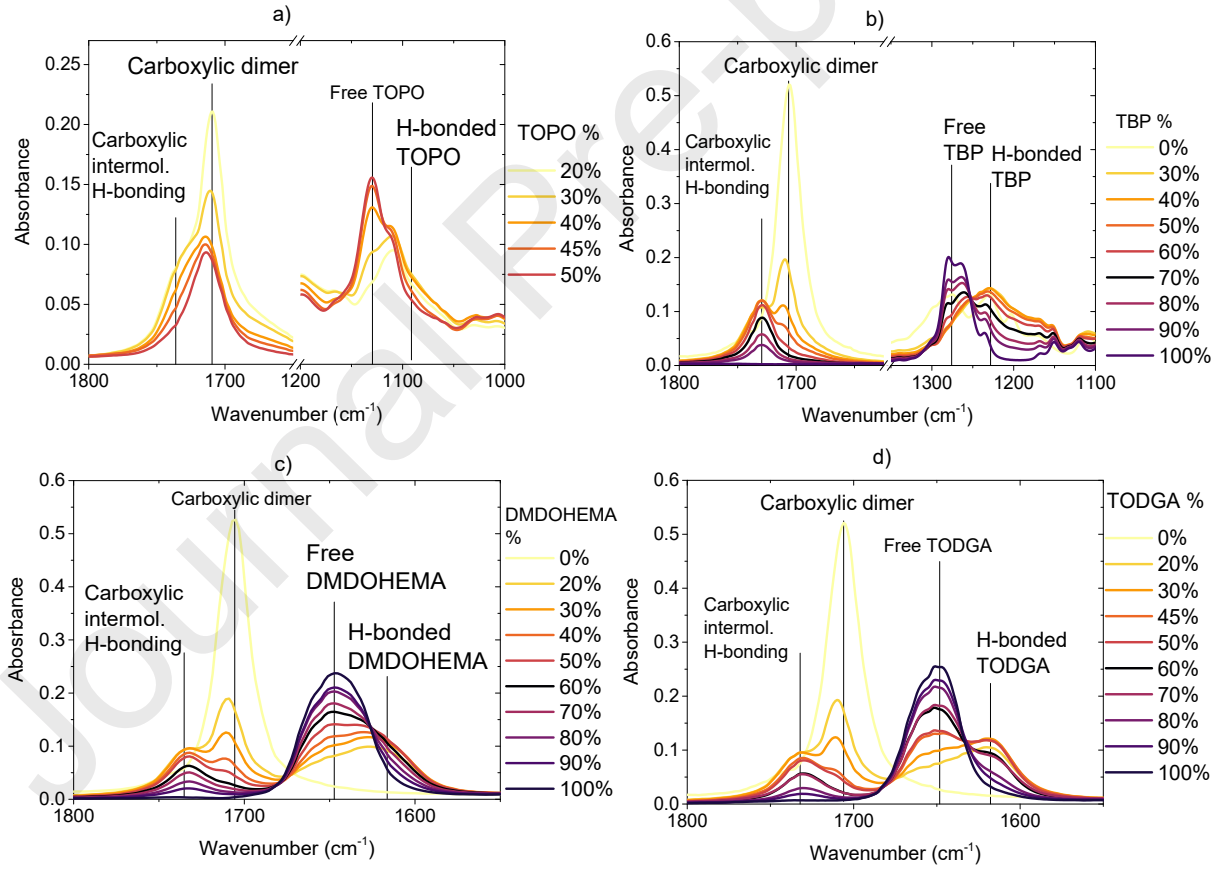

Figure 4: (a) Infrared spectra of TOPO + Decanoic acid system (b) TBP + Decanoic acid system (c) DMDOHEMA Decanoic acid system, and the (d) TODGA Decanoic acid system as a function of the molar ratio. Only composition that were liquid at 20°C were analyzed.

As described by Vargas *et al.*[60], the interaction between TOPO and decanoic acid results from hydrogen bonding, between the P=O group of TOPO and the hydroxyl groups of decanoic acid (**Figure 4a**). This is highlighted by the emergence of a hydrogen-bonded TOPO peak at 1110 cm^{-1}, particularly

visible when TOPO predominates in the mixture and also the widening of the peak for the decanoic acid at 1730 cm^{-1} indicates the formation of hydrogen bonds between TOPO and decanoic acid notably seen for x_{TOPO} = 0.2 or 0.3 (**Figure 4a**). Relating this observation to SX, the increased incorporation of TOPO within a loose hydrogen bonded framework is consistent with the significantly hindered extraction capacity of this HDES for lanthanides and platinum group metals upon x_{TOPO} decrease from 0.5 to 0.3.[4], [60] This is most likely due to change in the HBD-extractant interaction at the expense of metal-extractant chelation, effectively reducing the number of available ligands with the change in the HDES composition. These results on the reported and applied TOPO/DecA extraction system demonstrate the need to understand the interactions in the media to account for the complex and non-linear extraction behaviour. The same spectroscopic approach is applied to the new system here described.

Evidence of hydrogen bonding between TBP and DecA is characterized by the shift of the characteristic bands of free TBP in the P=O stretching region, observed at 1280 and 1264 cm^{-1}, as the concentration of DecA increases (**Figure 4b**). This shift is concomitant with the emergence and increase of a band at 1230 cm^{-1}, corresponding to TBP bound to DecA between the hydroxyl groups of decanoic acid and the phosphate of the TBP. In the case of the DMDOHEMA or TODGA mixtures with DecA respectively (**Figure 4c-d**), the formation of hydrogen bonds between HBA and DecA is evidenced by the appearance of a band between 1610 to 1620 cm^{-1} with increasing DecA molar fraction [61] corresponding to the H-bonded carbonyl C=O group of each extractant. Correspondingly, this is accompanied with the decrease of the band signature associated with the undiluted extractant molecules, here considered as non-hydrogen bonded, at approximately 1650 cm^{-1}. For the different composition, no significant changes are observed in the C-O-C bond of either DMDOHEMA or TODGA (**Figure S8 and S9**), indicating that the ether function remains uninvolved in the interaction with DecA. In all studied systems, bands from to carboxylic dimer at 1710 cm^{-1} decrease in intensity with increasing HBA concentration, substituted by bands assigned to carboxylic intermolecular hydrogen bonding at 1733 cm^{-1}.

To complete the infrared results, a Gaussian deconvolution was performed on the specific FT-IR bands of the four studied HDES systems to estimate the population of free and hydrogen bonded HBA, as well as dimeric and intermolecularly hydrogen bonded decanoic acid. An example of the peak deconvolution for each system is shown in **Figures S10** to **S14**. The full results are available in **Figure S15** to **S18** of the ESI, whilst the population of the H-bonded HBA in the four studied systems is presented in **Figure 5**. Whilst small differences are observable between systems, namely the greater population of H-bonded HBA for TOPO and TBP at lower x_{HBA} relative to the systems with DMODHEMA or TODGA, a rather gradual evolution of the hydrogen bonded population can be observed upon variation of the composition. The obtained results demonstrate two noteworthy aspects. Firstly, the predictable variation in the hydrogen bonding network of the mixtures indicates the absence of a magic composition at the eutectic composition. This is expectable as the SLE non-ideality does not provide any information regarding any potential non-ideality in the liquid phase, particularly for compositions studied at temperatures far above the SLE temperatures due to the temperature dependency of hydrogen bonding. Secondly, it is important to explicitly account for the concentration of free versus bound extractant when applying HDES at a fixed composition due to potential anti-synergistic effects on metal extraction arising from a greater fraction of hydrogen bonded extractants.

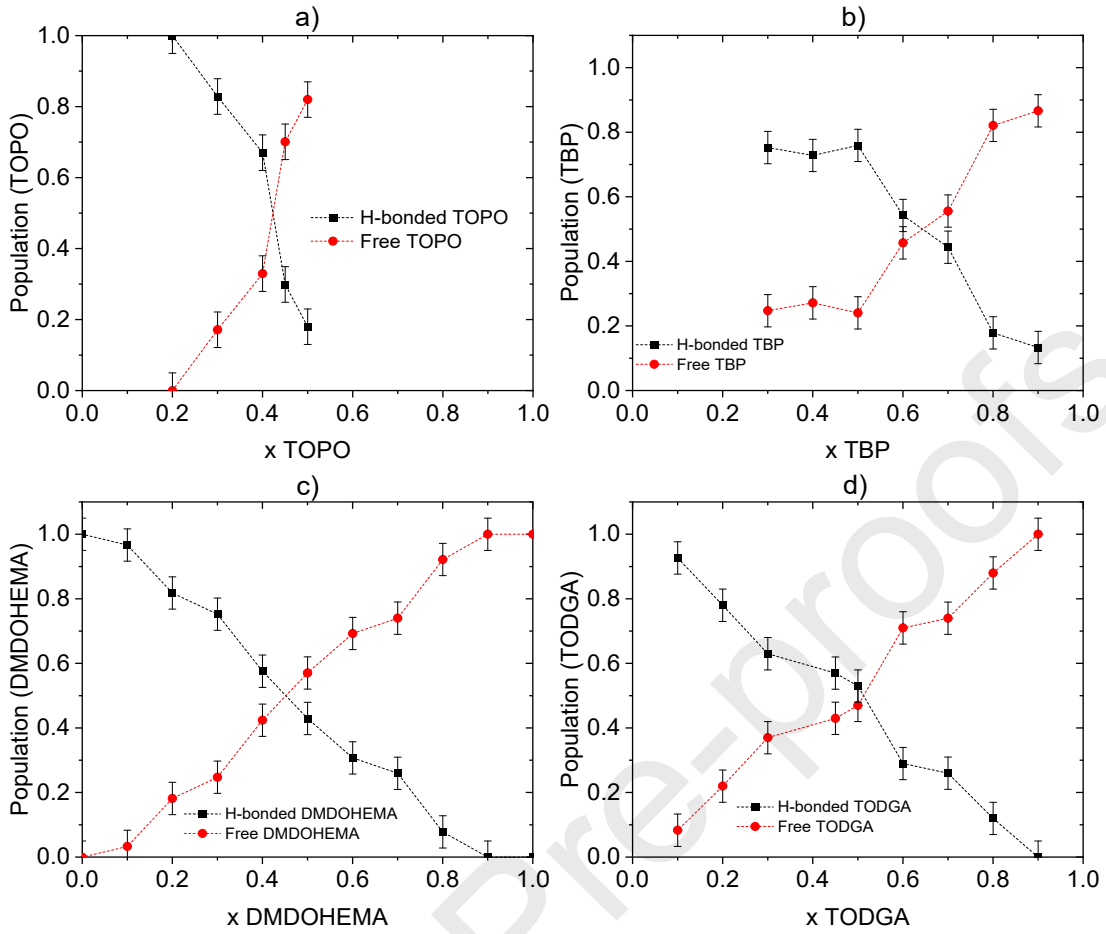

Figure 5: Distribution of hydrogen bonded (black) and free (red) HBA species in the HBA+Decanoic acid eutectic systems as a function of the composition. The relative population was derived from the integration of the FTIR bands presented in Figure 3. Only compopositions liquid at room temperature were investigated; octanoic acid instead of decanoic acid was used to determine the population at x_{HBA}=0. Deconvoluted peak areas used in the determination of the H-bonded population is available in **Table S3**.

c) Liquid phase structuring of HDES – influence of the HBA

To complete the understanding of the HDES liquid structuring, Small Angle X-rays Scattering experiments (SAXS) were performed, with the results presented in **Figure 6**. SAXS relies on the difference in the scattering of X-rays due to the aggregation of electron rich molecular groups such as the polar headgroups of the extractant relative to the surrounding electron poor such as the alkyl chains. It therefore provides information on the structuration of these system and the presence (or absence) of structured phases and aggregates at the nanometer scale. To simplify the comparison and reduce the number of systems, a fixed composition of x_{DecA}=0.7 was used for all mixtures with the aim of first determining the influence of the HBA on the liquid phase organization.

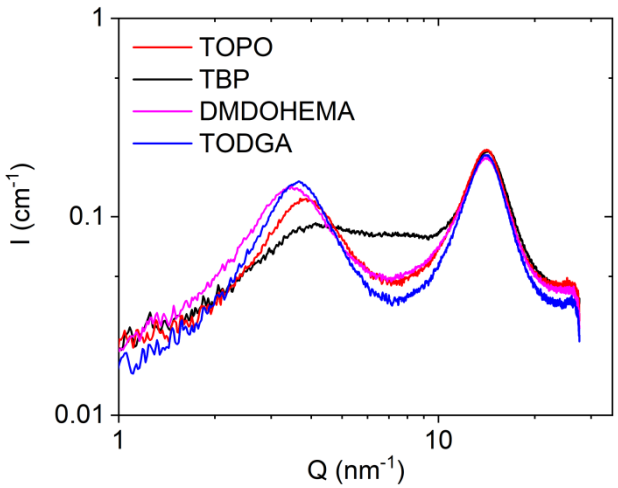

Figure 6: X-rays scattering profile for TBP, TOPO, TODGA or DMDOHEMA with Decanoic acid for a fixed HDES composition of $x_{DecAt} = 0.7$

Figure 6 shows that the as-prepared HDES containing TOPO, DMDOHEMA, and TODGA display a similar profile with two correlation peaks: a pre-peak centered at approximately 3.4 nm^{-1} for DMDOHEMA and TODGA and at 3.8 nm^{-1} for TOPO related to the nanoscale H-bond network, and a second at 13.9 nm^{-1} resulting from correlation between neighboring atoms. The pre-peak results from intermolecular interactions between two polar domains separated by the interpenetrating alkyl chains[4]. The second peak, also called solvent peak, is superposed for the four systems. It is assigned to C-C correlation distance which are the same for the four different extractant molecules. A comparison between the different systems reveals that DMDOHEMA, TODGA and TOPO show striking structural similarities in terms of their SAXS profile, with the pre-peak Q value corresponding to a real-space distance of 17.0 Å. This represents approximately 1.9x the length of octyl alkyl chain of TOPO or TODGA in a fully trans configuration (~9.0 Å), or 1.5x the length of decane alkyl chain of DecA (~11.5 Å), indicating the interdigitation of aliphatic domains between cluster for all three HDES. Importantly, no scattering is observed at lower Q values < 0.1 Å, confirming the absence of large-scale domains and the homogeneous structure of these HDES at the mesoscale. For the TBP system the pre-peak is shifted compared to the other systems and appears as a relatively wide peak. The pre-peak shift in the TBP system is attributed to the shorter butyl alkyl chains compared to the octyl chains of the other extractants. Distance between two polar groups is therefore reduced and leads to a shift to wider angles of the pre peak. This can lead to a change in the nature of polar domains due to easier intercalation and lower steric hindrance caused by the large difference in alkyl chain length between TBP and DecA when compared to the other HBAs used here.

To gain deeper insights into the spatial arrangement and interactions within HDES, SAXS measurements were coupled with MD simulations. These complementary techniques are particularly well-suited for examining the structural organization of complex fluids like HDES. SAXS, being highly sensitive to electron density contrasts, generates spectra that reveal the spatial organization of HDES components and their mutual interactions. However, since no direct analytical equations allow analyzing such systems, the structural description is typically derived by comparing experimental SAXS spectra with those calculated from MD simulations. Importantly, MD simulation outputs were compared against the experimental densities (**Table S4**) and SAXS profiles (**Figures S19-S22**), showing an excellent agreement. The final simulation snapshot for each system is presented in **Figure S23**. All simulations display the presence of discreet polar aggregates with mixed aggregates of extractants and decanoic acid as well as clusters of extractant only and carboxylic dimers.

Visually, TBP appears more aggregated compared to the other systems. This may be due to the polar head group of TBP, which represents a larger volume fraction of the molecule compared to the three others. TODGA, TOPO and DMDOHEMA have longer alkyl chains compared to the three butyl chains of the TBP, which translate to a more aggregated system.

To better understand the differences between the four systems, radial distribution functions (RDFs), coordination numbers (CNs), and hydrogen bond numbers (HBs) were computed as well as domain analysis to appreciate the segregation between polar domains (taken as the polar head groups of the extractant and decanoic acid) and apolar domains (taken as the alkyl chain). RDF and CN numbers are presented in **Figure 7**, between the H atom of the COOH group for DecA and the most probable oxygen HBA site for each extractant (P=O bond for TOPO and TBP; C=O carbonyl bond for DMDOHEMA and TODGA). All RDFs present an important g(r) peak at 0.19 to 0.20 nm, with no observable longer range structuring. The maximum of the g(r) peak for each system indicates a decreasing order of preferential interaction between DecA and the HBAs proceeding as TOPO > TBP > DMDOHEMA > TODGA, which is mirrored in the CN values at 0.20 nm. Interestingly, the observed sequence by MD follows the same qualitative trend as the extent of deviations to ideality in the phase diagrams presented in **Figure 2** further confirming stronger inter-component hydrogen bonding as the enthalpic driver for DES formation. Of added interest is the fact that a greater dentation of the HBA, if close together such that steric effect is the limiting factor for hydrogen bonding compounded by delocalization of the oxygen partial charge, appears to negatively affect the hydrogen bond strength and therefore DES formation.

The spatial distribution function of decanoic acid polar head around each HBA molecule is shown in **Figure 8**, with that of DMDOHEMA and TODGA differing from the monodentate TOPO and TBP. The more flexible DMDOHEMA and TODGA polar head is twisted, with each carbonyl bond pointing in contrary directions to maximize potential hydrogen bonding interactions by minimizing steric repulsion. A similar geometry was extracted from the optimized geometries (COSMO solvation model) of the interaction pairs recognized by COSMO-RS as most probable to be found in each respective mixture (**Figure S24**).

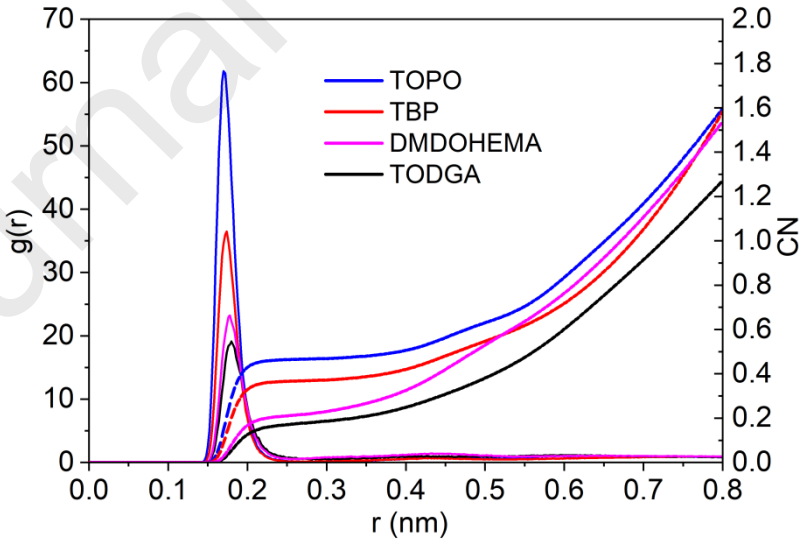

Figure 7: Radial distribution function and coordination number comparison between TOPO,TBP TODGA and DMDOHEMA+ Decanoic acid $x_{extractant}$ = 0.3

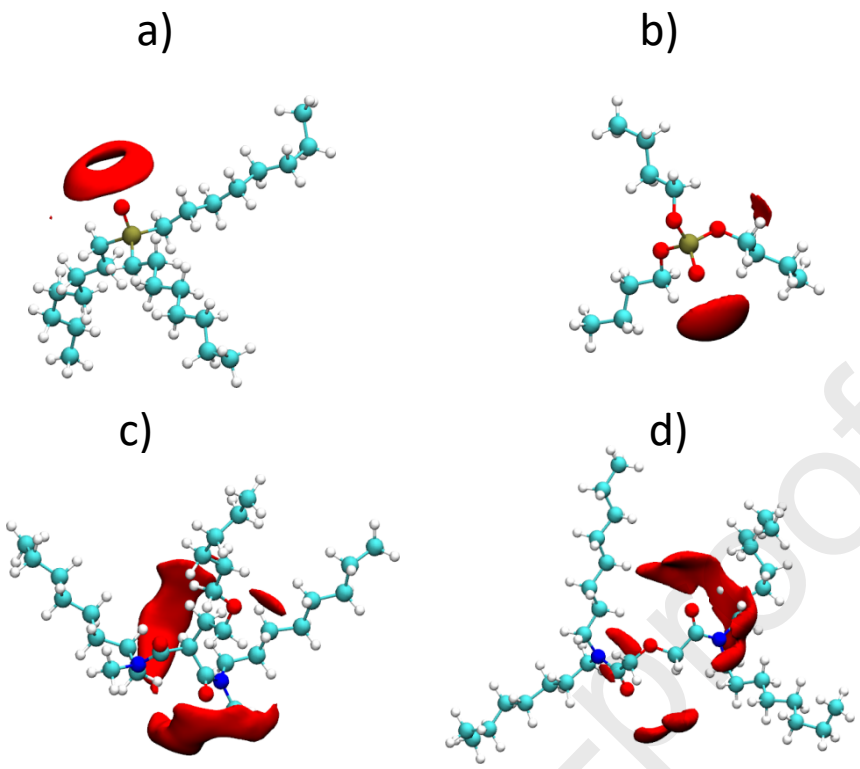

Figure 8: Spatial distribution function of a) TOPO + DecA b) TBP + DecA c) DMDOHEMA + DecA and d) TODGA + DecA, the red area corresponds to the polar head group of Decanoic acid

MD results were further exploited to analyze the H bond interactions in the four HDES systems, shown in **Figure 9**. Hydrogen bond distance and angle cut-off of 0.35 nm and 30° respectively were applied. **Figure 9a** reveals a more balanced system in terms of carboxylic dimers and intermolecular H-bond numbers for TOPO:DecA and DMDOHEMA:DecA compared to the two others systems based on TBP and TODGA. The number of hydrogen bonds between DMDOHEMA and DecA, is attributable to the partial involvement of the ether function of DMDOHEMA in the interaction between donor and acceptor as shown in **Figure 7**, a feature which is absent in the TODGA system. These results, which are also reported in **Table 3**, confirm the results obtained from infrared spectroscopy (**Figure 4**). This quantitative information also confirms the robustness, and the efficiency of the MD models employed in this study.

Table 3: Percentage of carboxylic dimers and intermolecular H-bonding derived from MD or FT-IR analysis for a x_{DecA} molar fraction of 0.7

System	% HBD dimer (MD)	% HBA-HBD (MD)	% HBD dimer (FTIR)	% HBA-HBD (FTIR)
TOPO + DecA	0.58	0.42	0.57	0.43
TBP + DecA	0.64	0.36	0.61	0.39
DMDOHEMA + DecA	0.53	0.47	0.52	0.48
TODGA + DecA	0.64	0.36	0.59	0.41

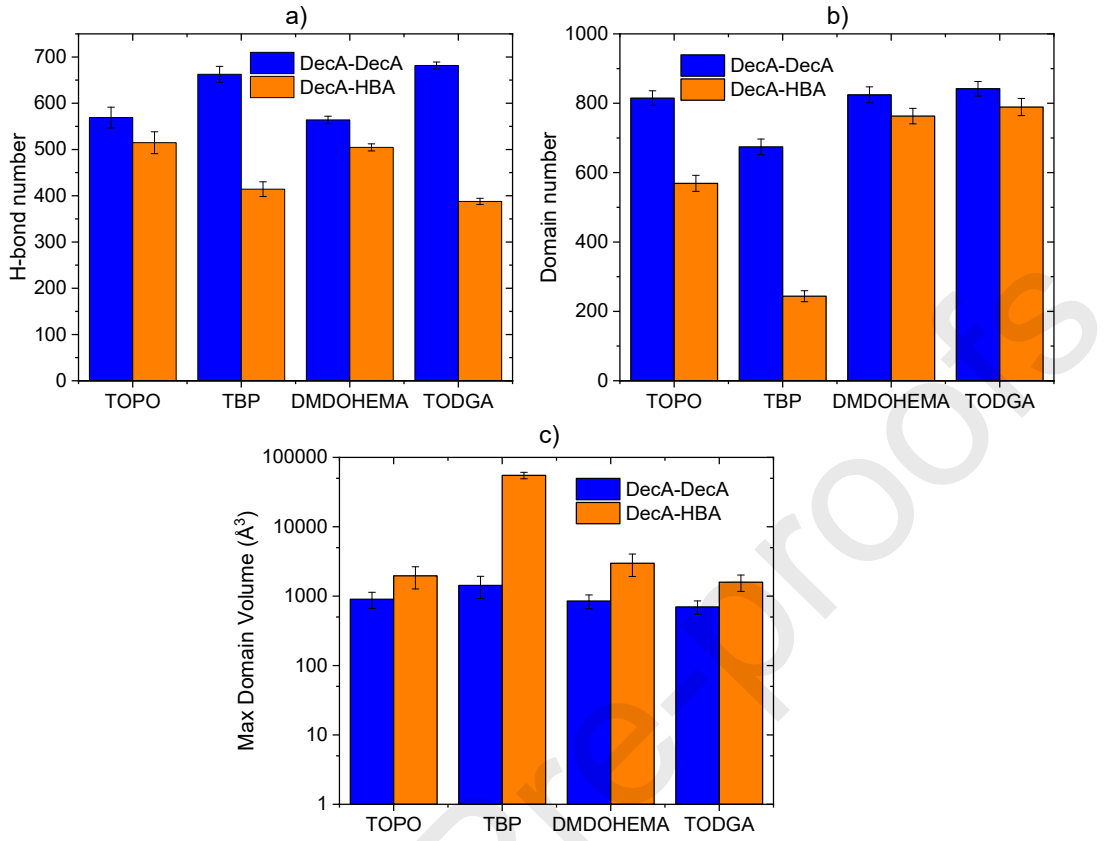

Figure 9: a) H-bond number, b) Domain number, and c) Maximum domain volume comparison between TOPO, TBP TODGA and DMDOHEMA + Decanoic acid for a fixed composition of $x_{DecA} = 0.70$

The decomposition of the liquid into domains of different subsets was followed by radical Voronoi tessellation. This led to useful averages of the subset neighbor count, i.e., the domain count, which gives the number of particular domains in the liquid **(Figure 9b**). Segregated domains can be identified by domain numbers greater than one, whereas a domain number of one represents continuous and uninterrupted domains. Notably, despite similar domain numbers between DMDOHEMA and TODGA systems, variations in RDF and SAXS spectra can be attributed to these differences. A small number of domains in the liquid phase corresponds to larger volumes for these phases as seen for the TBP system (**Figure 9b**). It is also interesting to consider that an increase of domain number may also increase segregation in the system which can affect the SAXS spectrum, as in **Figure 6**. The pre peak for the TBP decanoic acid system shifts to wider angles compared to TOPO, TOGDA or DMDOHEMA system, as smaller object scatters in the wider Q range. The lower domain number for the TBP system indicates therefore a decrease in the segregation in the system.

d) Liquid phase structuring of HDES – Influence of the molar fraction

Having ascertained the impact of HBA nature on the HDES structure, attention is paid to the influence of the molar fraction for a given HDES. The latter is an important but often overlooked parameter in the application of HDES, providing an extra degree of freedom for the optimization of their application. Given that there are no “magic compositions”[62] for which a marked special behavior is observable in the HDES at the microscopic level, valorizing the full liquidus composition range permits to fine tune solvent parameters of interest such as viscosity, density, or solvatochromic parameters [63]. Due to large

number of possible systems, the SAXS and MD analysis was restricted to the TODGA + DecA system for the ratio: x_{TODGA} = 0.30; 0.45 or 0.70. However, it expected that the derived conclusions are applicable to the other HDES under study considering their similar behavior with varying composition (see FTIR study, **Figure 5**). The experimental SAXS spectra of the systems is presented in **Figure 10** and SAXS profiles obtained by MD simulations in **Figure S22, S25** and **S26**. Regardless of the TODGA molar fraction, SAXS profile does not indicate any low q scattering, indicating a homogeneous dispersion and the absence of a large-scale structural heterogeneities. An increase of the TODGA molar fraction does not affect the adjacent peak but a shift to lower Q values is observed for the pre-peak, indicative of more distant polar domains. Nevertheless, no significant changes are observable, suggesting that the dominant features of the HDES structure are essentially constant across the composition range.

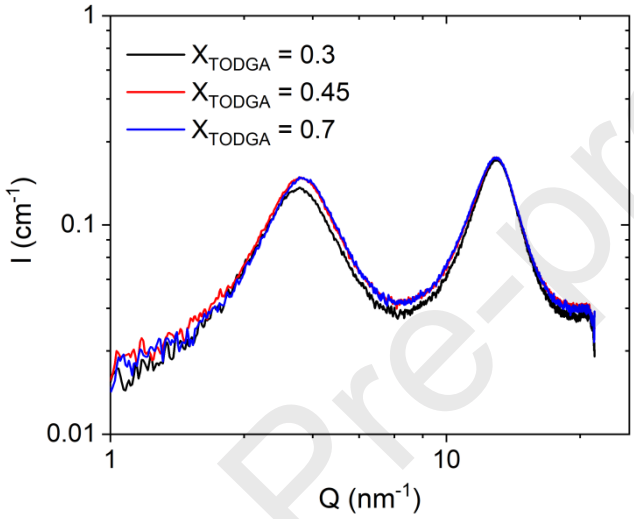

Figure 10: SAXS spectrum of TODGA + Decanoic acid for x_{TODGA} = 0.3; 0.45; 0.7

RDF results using the same reference atoms as in the previous section, available in **Figure S27** to **S29**, show that the preferential carboxylic acid interaction is through the formation of dimeric species, followed by hydrogen bonding with TODGA via the carbonyl C=O group, with minor interactions with the ether moiety of the TODGA head group independent of the HDES composition. The RDF profiles are consistent across the studied compositions, in line with the SAXS results, highlighting the unchanging nature of the primary intermolecular interactions in the mixtures. The results are particularly relevant to SX application as it suggests that in the case of this specific HDES mixture, the molar composition can be adjusted to reduce the TODGA molar fraction, the latter being more costly and viscous that fatty acids, without losing the metal extraction capability.

Hydrogen bond and domain analysis of the MD simulations indicate that reducing the amount of DecA in the system results in a decrease in the number of carboxylic acid dimers (**Table 4**) and consequently in a decrease in the total number of hydrogen bonds in the system, as shown in **Figure 11**, and also in a lower domain number. For higher TODGA percentages, the number of free TODGA molecules increases consistently with FT-IR results (**Table 4**). It leads also to smaller and more dispersed aggregates. For close to equimolar compositions (which corresponds to x_{TODGA} = 0.45), the system is characterized by a more balanced H-bond distribution but with less strong hydrogen bonds, and a similar amount of inter-component H-bonds despite more TODGA molecules are present.

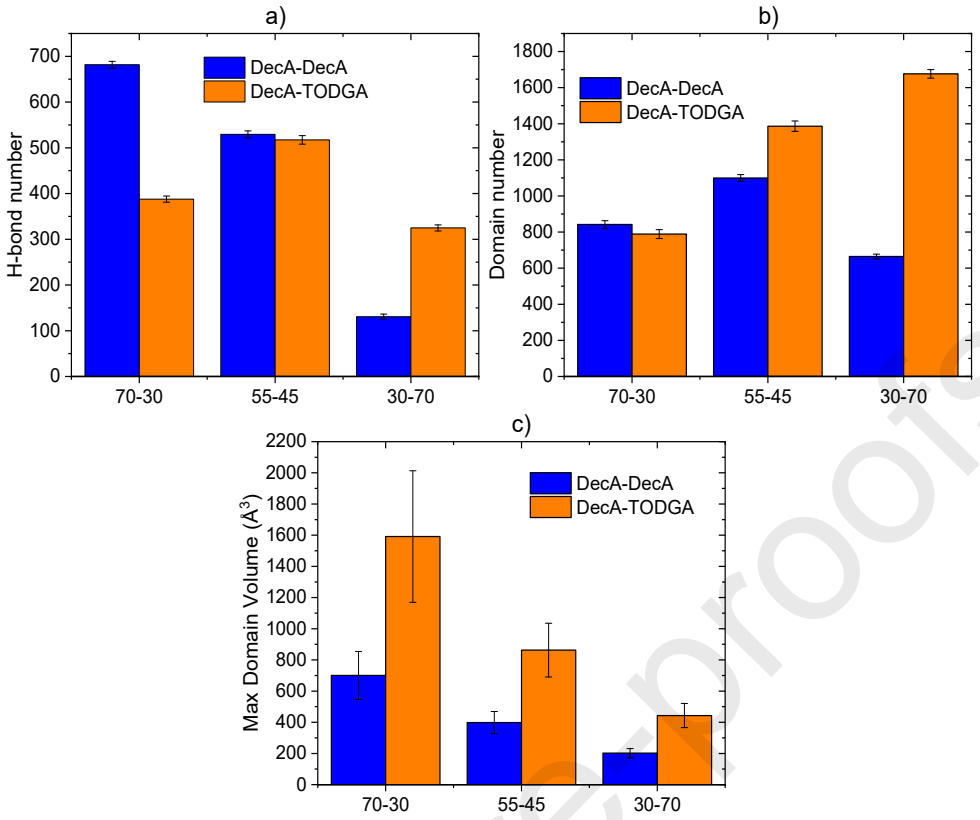

Figure 11: a) H-bond number and b) Domain number for three ratio and c) Maximum domain volume for three ratio of TODGA in TODGA decanoic acid system, in order x_{TODGA} = 0.3;0.45;0.7

Table 4: Comparison of the percentage of carboxylic dimers and intermolecular H-bonding for different ratio of TODGA and Decanoic acid between molecular dynamics and infrared

x_{TODGA}	% HBD dimer (MD)	% HBA-HBD (MD)	% HBD dimer (FTIR)	% HBA-HBD (FTIR)
0.30	0.64	0.36	0.59	0.41
0.45	0.53	0.47	0.51	0.49
0.70	0.26	0.74	0.27	0.73

e) Physico-chemical Properties

To highlight the potential application of these HDES systems as organic phases in a liquid-liquid extraction process, physico-chemicals properties such as density, viscosity and water solubility were determined. The viscosity at 25°C as a function of the HDES molar fraction for the four studied system is presented in **Figure 12.** Density and water solubilities were found to not vary significantly with the ratio x_{DecA}. They are therefore summarized in **Table 5** for a fixed ratio x_{DecA}=0.7. A linear increase in viscosity (**Figure 12**) was observed with increasing extractant content in the mixture, except for TBP which showed a slight decrease. For the system with TOPO, DMDOHEMA and TODGA we can see an increase of the viscosity with a decrease in the DecA molar fraction, corresponding to an approximate four-fold increase in the viscosity from x_{DecA} = 0.8 to 0.1 in the DMODHEMA and TODGA systems. This is consistent with the greater viscosity of these pure extracting being 125.8 and 160.2 for DMODHEMA and TODGA, respectively. This increase in viscosity with the HBA percentage for TODGA, DMDOHEMA, and TOPO can be attributed to greater molecular congestion and entanglement, resulting from their long alkyl chains compared to the HBD decanoic acid they are mixed

with. The enhanced chain interactions lead to a denser system with reduced molecular mobility, which ultimately causes the observed increase in viscosity. Conversely, the opposite phenomenon observed for TBP can be explained by its shorter alkyl chains relative to decanoic acid. This results in reduced molecular entanglement and, consequently, a decrease in viscosity as the TBP percentage increases. The viscosities are comparable to those of HDES reported in the literature [64], [65], which are much lower than hydrophilic DES and HDES based on quaternary ammonium salts. The changes in viscosity depend on the HBA components, the viscosity increases as follows: TBP< DMDOHEMA≈TODGA, as well as with increasing the molar fraction of extractant in the HDES system with the exception of TBP. Using the physicochemical data obtained, we can gain further insights into the type of system suitable as an organic phase for solvent extraction. These properties are inherent to the mixture and are independent of the depth of the eutectic solvent. As illustrated in **Figure 2**, although TOPO+DecA is the deepest eutectic solvent among the four systems, it is not the most viscous despite the stronger intermolecular hydrogen bonds. The most viscous system contains the greatest concentration of TODGA. When comparing the four systems with the same composition, viscosity is more influenced by the length of the alkyl chains. TODGA, with its four octyl chains, is more viscous than TOPO, which has three octyl chains, and TBP, which has three butyl chains is the least viscous. Viscosity is a critical parameter for future applications and must be low enough to facilitate experimental handling and allow spontaneous and rapid separation and mass transfer from the aqueous to the organic phases.

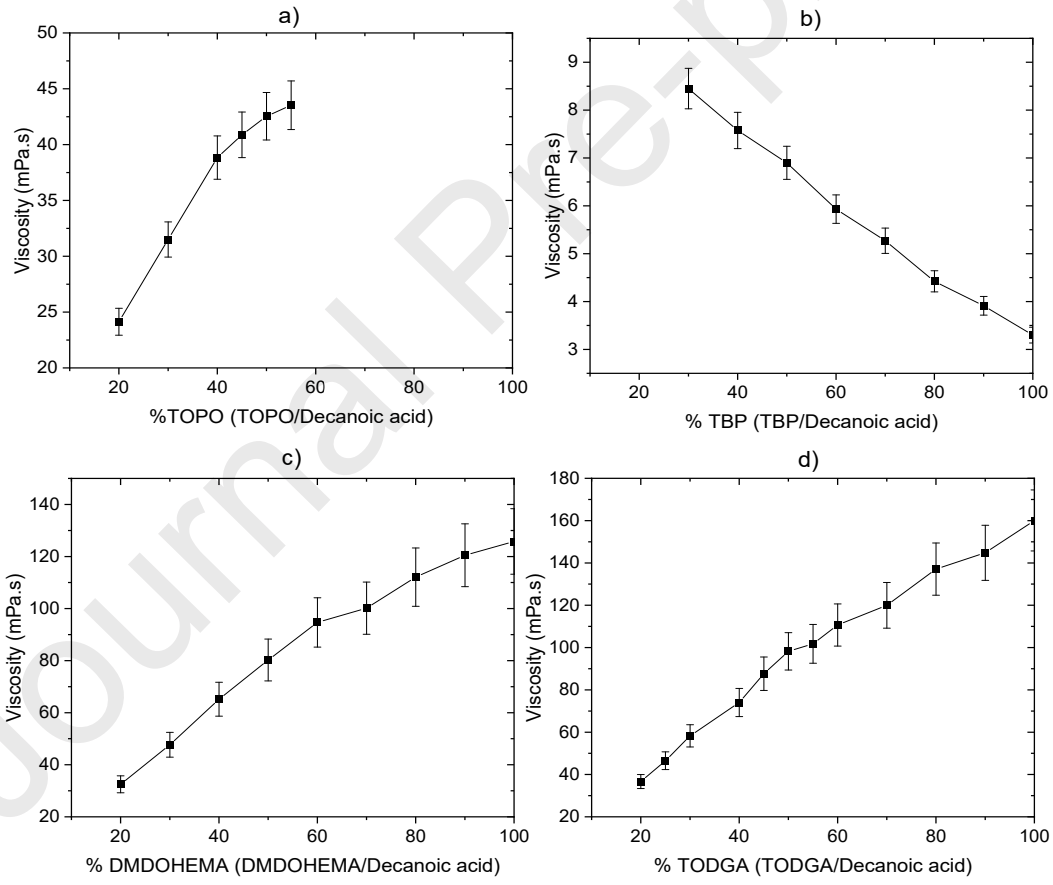

Figure 12: Viscosity of the as-prepared HDES at 25°C for (a) TOPO + Decanoic acid (b) TBP + Decanoic acid (c) DMDOHEMA + Decanoic acid and (d) TODGA + Decanoic acid system as a function of the mixture molar fraction.

The reported density and viscosity values in **Table 5** for selected systems investigated confirm that a phase separation between the HDES and an aqueous phase is possible, critical for their application as it for liquid-liquid extraction. The different HDES have similar density values around 0.9 $g.cm^{-3}$, which is lower than that of water, particularly when acidified, thereby facilitating phase demixing. For all five

systems, the total organic content in the aqueous phase after contact with water is low, clearly indicating the hydrophobic nature of the system with a very low solubility in water. Considering the use of hydrophobic HDES as extracting phase for solutes from aqueous phases, maintaining the chemical integrity of these HDES and their low water solubility is crucial. This includes preventing any contamination of the aqueous phase and minimizing the loss of HDES. Typically, the HDES studied have low solubility in water, lower than the equivalent conventional SX system of TODGA in dodecane with octanol, ranging from 0.019% to 0.039%. This low solubility is critical from both environmental and economic considerations, as it minimizes organic phase loss and improves recyclability. In an ideal solvent extraction process, the loss of organic phase to the aqueous phase should be negligible to prevent contamination and maintain the recyclability of the process. In the reference system for TODGA, the loss of organic phase to the aqueous phase is 0.051%, which is considerably low. The HDES system demonstrates a comparable magnitude of loss, within the margin of experimental error, which is promising for potential future applications. In summary, these systems have physico-chemicals properties that make them suitable for liquid-liquid extraction especially when compared to classic systems such TODGA 0.25 mol/L in dodecane octanol (5% v/v). For the different hydrophobic deep eutectic solvent (HDES) systems, there are minimal differences in terms of loss to the aqueous phase and water extraction. Therefore, to select the optimal system for use as the organic phase in solvent extraction, additional parameters should be considered. These include toxicity for environmental concerns and, more significantly, volatility both in terms of environmental impact to produce fewer volatile organic compounds and economic considerations. Less volatile compounds improve the recyclability of the process. The selection of the optimal system requires a compromise between all these parameters.

Table 5: Density, viscosity and total organic content after contact with water for the different HDES systems

System	Density (g/cm^3)	Viscosity (mPa.s)	% Loss of organic phase	% Water after contact (% wt)
TODGA 0.25 mol/L in dodecane octanol (5% v/v)	**0.775**	**2.29**	**0.051**	**0.31**
TOPO DecA , x_{TOPO} = 0.30	**0.886**	**31.5**	**0.039**	**2.36**
TBP DecA, $x_{TBP} = 0.30$	**0.925**	**8.5**	**0.034**	**3.81**
DMDOHEMA DecA , $x_{DMDOHEMA} = 0.30$	**0.913**	**47.7**	**0.04**	**4.84**
TODGA DecA, $x_{TODGA} = 0.30$	**0.907**	**58.3**	**0.016**	**3.22**
TODGA DecA, $x_{TODGA} = 0.45$	**0.905**	**87.7**	**0.019**	**2.69**
TODGA DecA, $x_{TODGA} = 0.70$	**0.904**	**120**	**0.019**	**2.35**

4. Conclusion

This study proposes an original exploration of non-ionic hydrophobic deep eutectic solvents (HDES) for optimized metal extraction applications. By systematically investigating mixtures between neutral extractants and decanoic acid, we successfully formed a series of neutral HDES systems with varied structural and physicochemical properties. The combination of Trioctylphosphine oxide (TOPO), Tributyl phosphate (TBP), *N,N′*-dimethyl,*N,N′*-dioctylhexylethoxymalonamide (DMDOHEMA), and *N,N,N′,N′*-tetraoctyl diglycolamide (TODGA) with decanoic acid (DecA) as a hydrogen bond donor (HBD) has led to the creation of several promising solvent systems, each displaying unique

characteristics in terms of phase behavior, hydrogen bonding, and structural organization which is important for further extraction experiments.

Detailed characterization by FT-IR spectroscopy, SAXS and MD simulations has led to a better understanding of the hydrogen bonding interactions underlying the formation of these HDES. Our results reveal that the nature of the hydrogen bond acceptor and the composition of the HDES significantly influence the phase behavior and physicochemical properties of the solvents. Phase diagrams and activity coefficients calculated by COSMO-RS and measured by DSC show significant deviations from ideal behavior, highlighting the complex H-bond interactions at play.

Our study confirms that HDES systems exhibit well-defined structural features at the nanoscale, with distinct hydrogen bond networks and domain structures that would be interesting to correlate with their extraction efficiency. Experimental results combined with computational models have elucidated the role of donors and acceptors groups. We have shown that variations in the molecular structure and composition of the extractant can fine-tune the physicochemical properties of HDES that are independent of the deepness of the HDES and the interaction that guide the HDES formation but more dependent on the structure of the starting components, leading to potential optimization route for applications in hydrometallurgy. Future research can build on these results to explore other extractant molecules, optimize solvent composition, and further investigate the potential of HDES. This includes an objective assessment of their challenges and limitations, such as economic and environmental costs associated with large-scale production, toxicity, volatility, and, most importantly, their scalability in various separation processes.

5. Acknowledgments

The authors would like to thank the French Government and ED 459 Sciences Chimiques Balard for the funding of the project and the attribution of PhD's fellowship and mobility grant. The authors are especially grateful to Amine GENESTE for DSC analyses in Montpellier. N.S. acknowledges the European Union for funding (ERC-StG, DESignSX-101116461). Views and opinions expressed are however those of the author only and do not necessarily reflect those of the European Union or the European Research Council. Neither the European Union nor the granting authority can be held responsible for them.

6. Conflict of interest

There are no conflicts of interest to declare.

7. Author contributions

B. Bernicot: Writing-original draft, Formal analysis and investigation, **G. Arrachart:**

Conceptualization, methodology, writing review and editing, supervisions **S. Dourdain**:

Conceptualization, methodology, writing review and editing, supervisions **N. Schaeffer**:

Conceptualization, methodology, data curation investigation, writing review and editing, supervisions

Gabriel Teixeira Santos: Data curation, formal analysis, investigations **S. Pellet-Rostaing** :

Conceptualization, funding acquisition, resources

8. Bibliography

[1] G. Arrachart, J. Couturier, S. Dourdain, C. Levard, et S. Pellet-Rostaing, « Recovery of Rare Earth Elements (REEs) Using Ionic Solvents », *Processes*, vol. 9, nº 7, p. 1202, juill. 2021, doi: 10.3390/pr9071202.

[2] M. C. Cann et M. E. Connelly, *Real-world Cases in Green Chemistry*. American Chemical Society, 2000.

[3] C. Molina, E. Quijada-Maldonado, J. Romero, et R. Abejón, « Neoteric Solvents for Rare Earths Processing: Perspectives on the Potential of Ionic Liquids and Deep Eutectic Solvents From a

Bibliometric Analysis », *Solvent Extr. Ion Exch.*, vol. 42, nº 6-7, p. 469-503, nov. 2024, doi: 10.1080/07366299.2024.2438700.
[4] U. G. Favero *et al.*, « Solvent extraction in non-ideal eutectic solvents – Application towards lanthanide separation », *Sep. Purif. Technol.*, vol. 314, p. 123592, juin 2023, doi: 10.1016/j.seppur.2023.123592.
[5] A. P. Abbott, D. Boothby, G. Capper, D. L. Davies, et R. K. Rasheed, « Deep Eutectic Solvents Formed between Choline Chloride and Carboxylic Acids: Versatile Alternatives to Ionic Liquids », *J. Am. Chem. Soc.*, vol. 126, nº 29, p. 9142-9147, juill. 2004, doi: 10.1021/ja048266j.
[6] B. B. Hansen *et al.*, « Deep Eutectic Solvents: A Review of Fundamentals and Applications », *Chem. Rev.*, vol. 121, nº 3, p. 1232-1285, févr. 2021, doi: 10.1021/acs.chemrev.0c00385.
[7] E. L. Smith, A. P. Abbott, et K. S. Ryder, « Deep Eutectic Solvents (DESs) and Their Applications », *Chem. Rev.*, vol. 114, nº 21, p. 11060-11082, nov. 2014, doi: 10.1021/cr300162p.
[8] N. Schaeffer *et al.*, « Non-Ideality in Thymol + Menthol Type V Deep Eutectic Solvents », *ACS Sustain. Chem. Eng.*, vol. 9, nº 5, p. 2203-2211, févr. 2021, doi: 10.1021/acssuschemeng.0c07874.
[9] D. J. G. P. van Osch, D. Parmentier, C. H. J. T. Dietz, A. van den Bruinhorst, R. Tuinier, et M. C. Kroon, « Removal of alkali and transition metal ions from water with hydrophobic deep eutectic solvents », *Chem. Commun.*, vol. 52, nº 80, p. 11987-11990, 2016, doi: 10.1039/C6CC06105B.
[10] D. J. G. P. van Osch, C. H. J. T. Dietz, S. E. E. Warrag, et M. C. Kroon, « The Curious Case of Hydrophobic Deep Eutectic Solvents: A Story on the Discovery, Design, and Applications », *ACS Sustain. Chem. Eng.*, p. acssuschemeng.0c00559, juill. 2020, doi: 10.1021/acssuschemeng.0c00559.
[11] S. Chen *et al.*, « Deep eutectic solvents for separation and purification applications in critical metal metallurgy: Recent advances and perspectives », *Int. J. Miner. Metall. Mater.*, vol. 32, nº 1, p. 1-19, janv. 2025, doi: 10.1007/s12613-024-2923-7.
[12] G. Zante et M. Boltoeva, « Review on Hydrometallurgical Recovery of Metals with Deep Eutectic Solvents », *Sustain. Chem.*, vol. 1, nº 3, p. 238-255, oct. 2020, doi: 10.3390/suschem1030016.
[13] E. E. Tereshatov, M. Yu. Boltoeva, et C. M. Folden, « First evidence of metal transfer into hydrophobic deep eutectic and low-transition-temperature mixtures: indium extraction from hydrochloric and oxalic acids », *Green Chem.*, vol. 18, nº 17, p. 4616-4622, 2016, doi: 10.1039/C5GC03080C.
[14] Y. Shi, D. Xiong, Y. Zhao, T. Li, K. Zhang, et J. Fan, « Highly efficient extraction/separation of Cr (VI) by a new family of hydrophobic deep eutectic solvents », *Chemosphere*, vol. 241, p. 125082, févr. 2020, doi: 10.1016/j.chemosphere.2019.125082.
[15] Y. Geng, Z. Xiang, C. Lv, N. Wang, Y. Wang, et Y. Yang, « Recovery of gold from hydrochloric medium by deep eutectic solvents based on quaternary ammonium salts », *Hydrometallurgy*, vol. 188, p. 264-271, sept. 2019, doi: 10.1016/j.hydromet.2019.06.013.
[16] O. Mokhodoeva, V. Maksimova, A. Shishov, et V. Shkinev, « Separation of platinum group metals using deep eutectic solvents based on quaternary ammonium salts », *Sep. Purif. Technol.*, vol. 305, p. 122427, janv. 2023, doi: 10.1016/j.seppur.2022.122427.
[17] K. Xue *et al.*, « Highly selective deep eutectic solvents for the recovery of lithium from high sodium concentration aqueous solutions », *AIChE J.*, p. e18679, janv. 2025, doi: 10.1002/aic.18679.
[18] D. O. Abranches et J. A. P. Coutinho, « Type V deep eutectic solvents: Design and applications », *Curr. Opin. Green Sustain. Chem.*, vol. 35, p. 100612, juin 2022, doi: 10.1016/j.cogsc.2022.100612.
[19] K. A. M. L. Cruz, F. R. P. Rocha, et M. C. Hespanhol, « Greener Route for Recovery of High-Purity Lanthanides from the Waste of Nickel Metal Hydride Battery Using a Hydrophobic Deep Eutectic Solvent », *ACS Sustain. Chem. Eng.*, vol. 12, nº 16, p. 6169-6181, avr. 2024, doi: 10.1021/acssuschemeng.3c07784.
[20] M. Gilmore, É. N. McCourt, F. Connolly, P. Nockemann, M. Swadźba-Kwaśny, et J. D. Holbrey, « Hydrophobic Deep Eutectic Solvents Incorporating Trioctylphosphine Oxide:

Advanced Liquid Extractants », *ACS Sustain. Chem. Eng.*, vol. 6, nº 12, p. 17323-17332, déc. 2018, doi: 10.1021/acssuschemeng.8b04843.
[21] N. Schaeffer *et al.*, « Non-ionic hydrophobic eutectics – versatile solvents for tailored metal separation and valorisation », *Green Chem.*, vol. 22, nº 9, p. 2810-2820, 2020, doi: 10.1039/D0GC00793E.
[22] K. George, A. J. Masters, F. R. Livens, M. J. Sarsfield, R. J. Taylor, et C. A. Sharrad, « A review of technetium and zirconium extraction into tributyl phosphate in the PUREX process », *Hydrometallurgy*, vol. 211, p. 105892, mai 2022, doi: 10.1016/j.hydromet.2022.105892.
[23] S. Panja, S. C. Tripathi, P. S. Dhami, et P. M. Gandhi, « Solvent Extraction of Pu(IV) using TBP : A comparative study of n-dodecane and a Room Temperature Ionic Liquid », *Sep. Sci. Technol.*, p. 150615133607009, juin 2015, doi: 10.1080/01496395.2015.1052883.
[24] O. Pecheur *et al.*, « Synergism in a HDEHP/TOPO Liquid–Liquid Extraction System: An Intrinsic Ligands Property? », *J. Phys. Chem. B*, vol. 120, nº 10, p. 2814-2823, mars 2016, doi: 10.1021/acs.jpcb.5b11693.
[25] A. Geist, L. Berthon, M.-C. Charbonnel, et U. Müllich, « Extraction of Nitric Acid, Americium(III), Curium(III), and Lanthanides(III) into DMDOHEMA Dissolved in Kerosene », *Solvent Extr. Ion Exch.*, vol. 38, nº 7, p. 681-702, nov. 2020, doi: 10.1080/07366299.2020.1794523.
[26] S. Chapron *et al.*, « Separation of Americium by Liquid-Liquid Extraction Using Diglycolamides Water-Soluble Complexing Agents », *Procedia Chem.*, vol. 21, p. 133-139, 2016, doi: 10.1016/j.proche.2016.10.019.
[27] C. L. Usma, S. Dourdain, G. Arrachart, et S. Pellet-Rostaing, « Solvent extraction of rare earths elements from nitrate media in DMDOHEMA/ionic liquid systems: performance and mechanism studies », *RSC Adv.*, vol. 11, nº 50, p. 31197-31207, 2021, doi: 10.1039/D1RA05359K.
[28] S. Hirata *et al.*, « Lanthanide and Actinide Ion Complexes Containing Organic Ligands Investigated by Surface-Enhanced Infrared Absorption Spectroscopy », *Inorg. Chem.*, vol. 62, nº 1, p. 474-486, janv. 2023, doi: 10.1021/acs.inorgchem.2c03618.
[29] A. Sengupta, Sk. M. Ali, et K. T. Shenoy, « Understanding the complexation of the Eu3+ ion with TODGA, CMPO, TOPO and DMDBTDMA: Extraction, luminescence and theoretical investigation », *Polyhedron*, vol. 117, p. 612-622, oct. 2016, doi: 10.1016/j.poly.2016.06.037.
[30] A. K. Dwamena, « Recent Advances in Hydrophobic Deep Eutectic Solvents for Extraction », *Separations*, vol. 6, nº 1, Art. nº 1, mars 2019, doi: 10.3390/separations6010009.
[31] S. Belfqueh, « Développement d'un procédé éco-compatible de recyclage des terres rares issues des aimants permanents », PhD Thesis, Montpellier University, Université de Montpellier, 2022.
[32] J. A. P. Coutinho, S. I. Andersen, et E. H. Stenby, « Evaluation of activity coefficient models in prediction of alkane solid-liquid equilibria », *Fluid Phase Equilibria*, vol. 103, nº 1, p. 23-39, janv. 1995, doi: 10.1016/0378-3812(94)02600-6.
[33] Prausnitz, J. M.; Lichtenthaler, R. N.; Azevedo, E.G, *Fluid-Phase Equilibria, 3rd ed*, Prentince Hall. Upper Saddle River, NJ.
[34] R. C. F. Schaake, J. C. van Miltenburg, et C. G. De Kruif, « Thermodynamic properties of the normal alkanoic acids II. Molar heat capacities of seven even-numbered normal alkanoic acids », *J. Chem. Thermodyn.*, vol. 14, nº 8, p. 771-778, août 1982, doi: 10.1016/0021-9614(82)90173-2.
[35] A. Klamt, « Conductor-like Screening Model for Real Solvents: A New Approach to the Quantitative Calculation of Solvation Phenomena », *J. Phys. Chem.*, vol. 99, nº 7, p. 2224-2235, févr. 1995, doi: 10.1021/j100007a062.
[36] H. F. Hizaddin, A. Ramalingam, M. A. Hashim, et M. K. O. Hadj-Kali, « Evaluating the Performance of Deep Eutectic Solvents for Use in Extractive Denitrification of Liquid Fuels by the Conductor-like Screening Model for Real Solvents », *J. Chem. Eng. Data*, vol. 59, nº 11, p. 3470-3487, nov. 2014, doi: 10.1021/je5004302.
[37] M. Abraham *et al.*, « GROMACS 2023 Manual », févr. 2023, doi: 10.5281/zenodo.7588711.
[38] R. W. Hockney, S. P. Goel, et J. W. Eastwood, « Quiet high-resolution computer models of a plasma », *J. Comput. Phys.*, vol. 14, nº 2, p. 148-158, févr. 1974, doi: 10.1016/0021-9991(74)90010-2.

[39] W. L. Jorgensen, D. S. Maxwell, et J. Tirado-Rives, « Development and Testing of the OPLS All-Atom Force Field on Conformational Energetics and Properties of Organic Liquids », *J. Am. Chem. Soc.*, vol. 118, nº 45, p. 11225-11236, nov. 1996, doi: 10.1021/ja9621760.
[40] L. S. Dodda, J. Z. Vilseck, J. Tirado-Rives, et W. L. Jorgensen, « 1.14*CM1A-LBCC: Localized Bond-Charge Corrected CM1A Charges for Condensed-Phase Simulations », *J. Phys. Chem. B*, vol. 121, nº 15, p. 3864-3870, avr. 2017, doi: 10.1021/acs.jpcb.7b00272.
[41] L. S. Dodda, I. Cabeza de Vaca, J. Tirado-Rives, et W. L. Jorgensen, « LigParGen web server: an automatic OPLS-AA parameter generator for organic ligands », *Nucleic Acids Res.*, vol. 45, nº W1, p. W331-W336, juill. 2017, doi: 10.1093/nar/gkx312.
[42] B. Hess, H. Bekker, H. J. C. Berendsen, et J. G. E. M. Fraaije, « LINCS: A linear constraint solver for molecular simulations », *J. Comput. Chem.*, vol. 18, nº 12, p. 1463-1472, 1997, doi: 10.1002/(SICI)1096-987X(199709)18:12<1463::AID-JCC4>3.0.CO;2-H.
[43] D. J. Evans et B. L. Holian, « The Nose–Hoover thermostat », *J. Chem. Phys.*, vol. 83, nº 8, p. 4069-4074, oct. 1985, doi: 10.1063/1.449071.
[44] M. Parrinello et A. Rahman, « Polymorphic transitions in single crystals: A new molecular dynamics method », *J. Appl. Phys.*, vol. 52, nº 12, p. 7182-7190, déc. 1981, doi: 10.1063/1.328693.
[45] W. Humphrey, A. Dalke, et K. Schulten, « VMD: Visual molecular dynamics », *J. Mol. Graph.*, vol. 14, nº 1, p. 33-38, févr. 1996, doi: 10.1016/0263-7855(96)00018-5.
[46] M. Brehm et B. Kirchner, « TRAVIS - A Free Analyzer and Visualizer for Monte Carlo and Molecular Dynamics Trajectories », *J. Chem. Inf. Model.*, vol. 51, nº 8, p. 2007-2023, août 2011, doi: 10.1021/ci200217w.
[47] M. Brehm, H. Weber, M. Thomas, O. Hollóczki, et B. Kirchner, « Domain Analysis in Nanostructured Liquids: A Post-Molecular Dynamics Study at the Example of Ionic Liquids », *ChemPhysChem*, vol. 16, nº 15, p. 3271-3277, 2015, doi: 10.1002/cphc.201500471.
[48] E. Moreno *et al.*, « Polymorphism of even saturated carboxylic acids from n-decanoic to n-eicosanoic acid », *New J. Chem.*, vol. 31, nº 6, p. 947-957, juin 2007, doi: 10.1039/B700551B.
[49] G. Mannucci *et al.*, « Predicting the Thermal Behavior in the Design of Type V Deep Eutectic Solvents: The Combined Role of Polarity and Steric Asymmetry », *ACS Sustain. Chem. Eng.*, vol. 12, nº 7, p. 2862-2870, févr. 2024, doi: 10.1021/acssuschemeng.3c07965.
[50] R. J. Ellis, T. L. Anderson, M. R. Antonio, A. Braatz, et M. Nilsson, « A SAXS Study of Aggregation in the Synergistic TBP–HDBP Solvent Extraction System », *J. Phys. Chem. B*, vol. 117, nº 19, p. 5916-5924, mai 2013, doi: 10.1021/jp401025e.
[51] Q. Sun, H. Chen, et J. Yu, « Investigation on the Lithium Extraction Process with the TBP–FeCl3 Solvent System Using Experimental and DFT Methods », *Ind. Eng. Chem. Res.*, vol. 61, nº 13, p. 4672-4682, avr. 2022, doi: 10.1021/acs.iecr.1c05072.
[52] D. Massey, A. Masters, J. Macdonald-Taylor, D. Woodhead, et R. Taylor, « Molecular Dynamics Study of the Aggregation Behavior of N,N,N′,N′-Tetraoctyl Diglycolamide », *J. Phys. Chem. B*, vol. 126, nº 33, p. 6290-6300, août 2022, doi: 10.1021/acs.jpcb.2c02198.
[53] A. van den Bruinhorst et M. Costa Gomes, « Is there depth to eutectic solvents? », *Curr. Opin. Green Sustain. Chem.*, vol. 37, p. 100659, oct. 2022, doi: 10.1016/j.cogsc.2022.100659.
[54] P. Tkac, G. F. Vandegrift, G. J. Lumetta, et A. V. Gelis, « Study of the Interaction between HDEHP and CMPO and Its Effect on the Extraction of Selected Lanthanides », *Ind. Eng. Chem. Res.*, vol. 51, nº 31, p. 10433-10444, août 2012, doi: 10.1021/ie300326d.
[55] J. Ferraro, M. Borkowski, R. Chiarizia, et D. McAlister, « FT-IR SPECTROSCOPY OF NITRIC ACID IN TBP/OCTANE SOLUTION1* », *Solvent Extr. Ion Exch.*, vol. 19, nº 6, p. 981-992, janv. 2001, doi: 10.1081/SEI-100107614.
[56] S. Murakami, M. Matsumiya, T. Yamada, et K. Tsunashima, « Extraction of Pr(III), Nd(III), and Dy(III) from HTFSA Aqueous Solution by TODGA/Phosphonium-Based Ionic Liquids », *Solvent Extr. Ion Exch.*, vol. 34, nº 2, p. 172-187, févr. 2016, doi: 10.1080/07366299.2016.1144951.
[57] E. L. Campbell, V. E. Holfeltz, G. B. Hall, K. L. Nash, G. J. Lumetta, et T. G. Levitskaia, « Nitric Acid and Water Extraction by T2EHDGA in *n* -Dodecane », *Solvent Extr. Ion Exch.*, vol. 35, nº 7, p. 586-603, nov. 2017, doi: 10.1080/07366299.2017.1400161.

[58] R. Poirot, D. Bourgeois, et D. Meyer, « Palladium Extraction by a Malonamide Derivative (DMDOHEMA) from Nitrate Media: Extraction Behavior and Third Phase Characterization », *Solvent Extr. Ion Exch.*, vol. 32, nº 5, p. 529-542, juill. 2014, doi: 10.1080/07366299.2014.908587.
[59] A. Filopoulou, S. Vlachou, et S. C. Boyatzis, « Fatty Acids and Their Metal Salts: A Review of Their Infrared Spectra in Light of Their Presence in Cultural Heritage », *Molecules*, vol. 26, nº 19, Art. nº 19, janv. 2021, doi: 10.3390/molecules26196005.
[60] S. J. R. Vargas, G. Pérez-Sánchez, N. Schaeffer, et J. A. P. Coutinho, « Solvent extraction in extended hydrogen bonded fluids – separation of Pt using TOPO-based type V DES », *Green Chem.*, vol. 23, nº 12, p. 4540-4550, 2021, doi: 10.1039/D1GC00829C.
[61] P. Narayanan, K. R. Swami, T. Prathibha, et K. A. Venkatesan, « FTIR spectroscopic investigations on the aggregation behaviour of N,N,N′,N′-tetraoctyldiglycolamide and N,N-dioctylhydroxyacetamide in n-dodecane during the extraction of Nd(III) from nitric acid medium », *J. Mol. Liq.*, vol. 314, p. 113685, sept. 2020, doi: 10.1016/j.molliq.2020.113685.
[62] V. Alizadeh, F. Malberg, A. A. H. Pádua, et B. Kirchner, « Are There Magic Compositions in Deep Eutectic Solvents? Effects of Composition and Water Content in Choline Chloride/Ethylene Glycol from Ab Initio Molecular Dynamics », *J. Phys. Chem. B*, vol. 124, nº 34, p. 7433-7443, août 2020, doi: 10.1021/acs.jpcb.0c04844.
[63] M. A. R. Martins *et al.*, « Greener Terpene–Terpene Eutectic Mixtures as Hydrophobic Solvents », *ACS Sustain. Chem. Eng.*, vol. 7, nº 20, p. 17414-17423, oct. 2019, doi: 10.1021/acssuschemeng.9b04614.
[64] C. Florindo, L. C. Branco, et I. M. Marrucho, « Quest for Green-Solvent Design: From Hydrophilic to Hydrophobic (Deep) Eutectic Solvents », *ChemSusChem*, vol. 12, nº 8, p. 1549-1559, 2019, doi: 10.1002/cssc.201900147.
[65] K. A. Omar et R. Sadeghi, « Database of deep eutectic solvents and their physical properties: A review », *J. Mol. Liq.*, vol. 384, p. 121899, août 2023, doi: 10.1016/j.molliq.2023.121899.

Author statement

B. Bernicot: Writing-original draft, Formal analysis and investigation, **G. Arrachart:**

Conceptualization, methodology, writing review and editing, supervisions **S. Dourdain**:

Conceptualization, methodology, writing review and editing, supervisions **N. Schaeffer**:

Conceptualization, methodology, data curation investigation, writing review and editing, supervisions

Gabriel Teixeira Santos: Data curation, formal analysis, investigations **S. Pellet-Rostaing** :

Conceptualization, funding acquisition, resources

Declaration of interests

☒ The authors declare that they have no known competing financial interests or personal relationships that could have appeared to influence the work reported in this paper.

☐ The authors declare the following financial interests/personal relationships which may be considered as potential competing interests:

Figure file

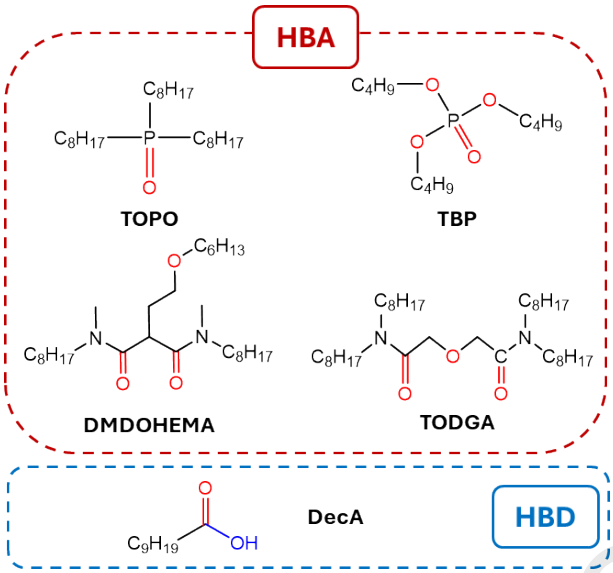

Figure 2: Structure and acronyms of the hydrogen bond acceptors (HBA) and donors (HBD) molecules used in this work, with the potential acceptor and donor sites highlighted in red and blue respectively.

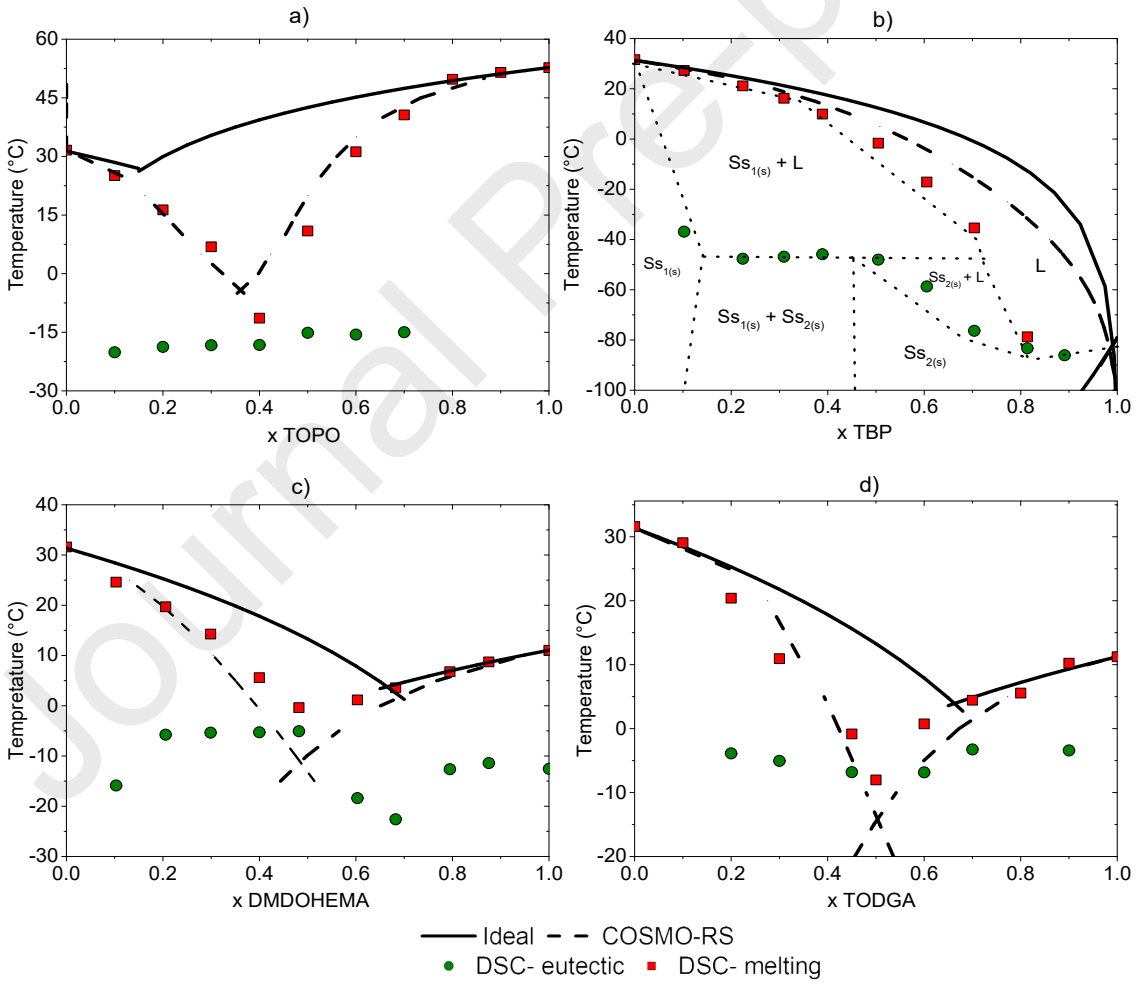

Figure 3: Phase diagram of (a) TOPO + Decanoic acid adapted from [15] (b) TBP + Decanoic acid (c) DMDOHEMA + Decanoic acid and (d) TODGA + Decanoic acid

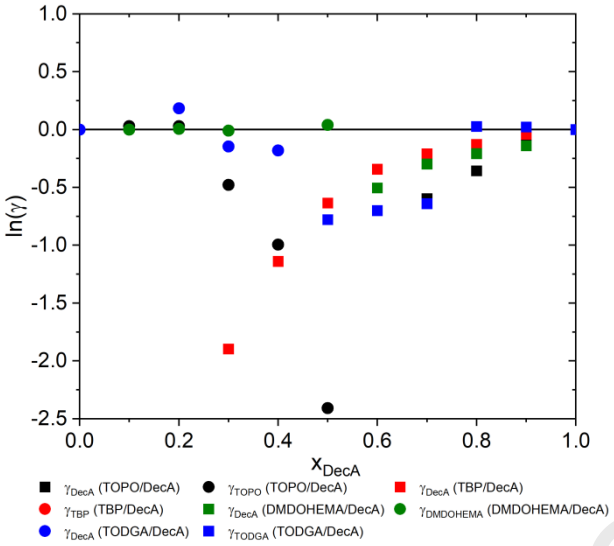

Figure 4: Non-isothermal activity coefficients of Decanoic acid with TOPO (black symbols), TBP (red symbols), DMDOHEMA (green symbols), TODGA (blue symbols) and TOPO, adapted from *[17]*. Symbols represent the activity coefficient of decanoid acid (squares) and the second compound (circle).

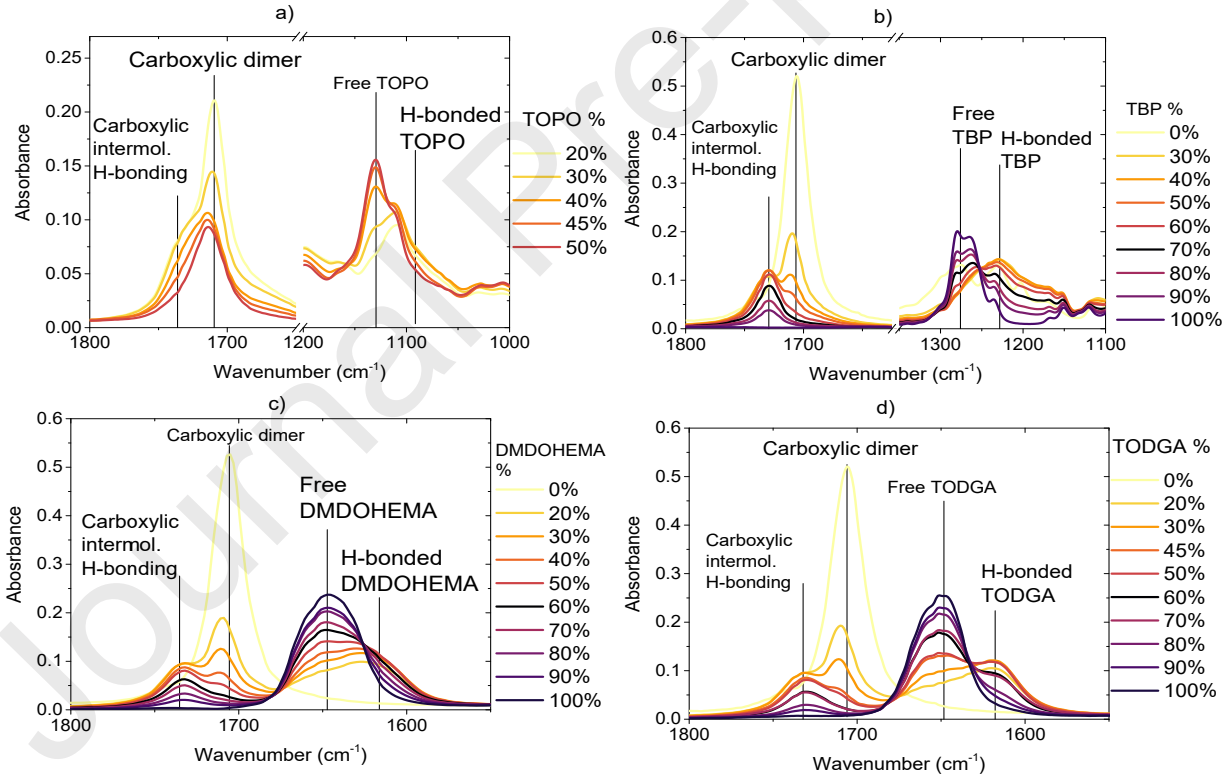

Figure 5: (a) Infrared spectra of TOPO + Decanoic acid system (b) TBP + Decanoic acid system (c) DMDOHEMA (d) TODGA

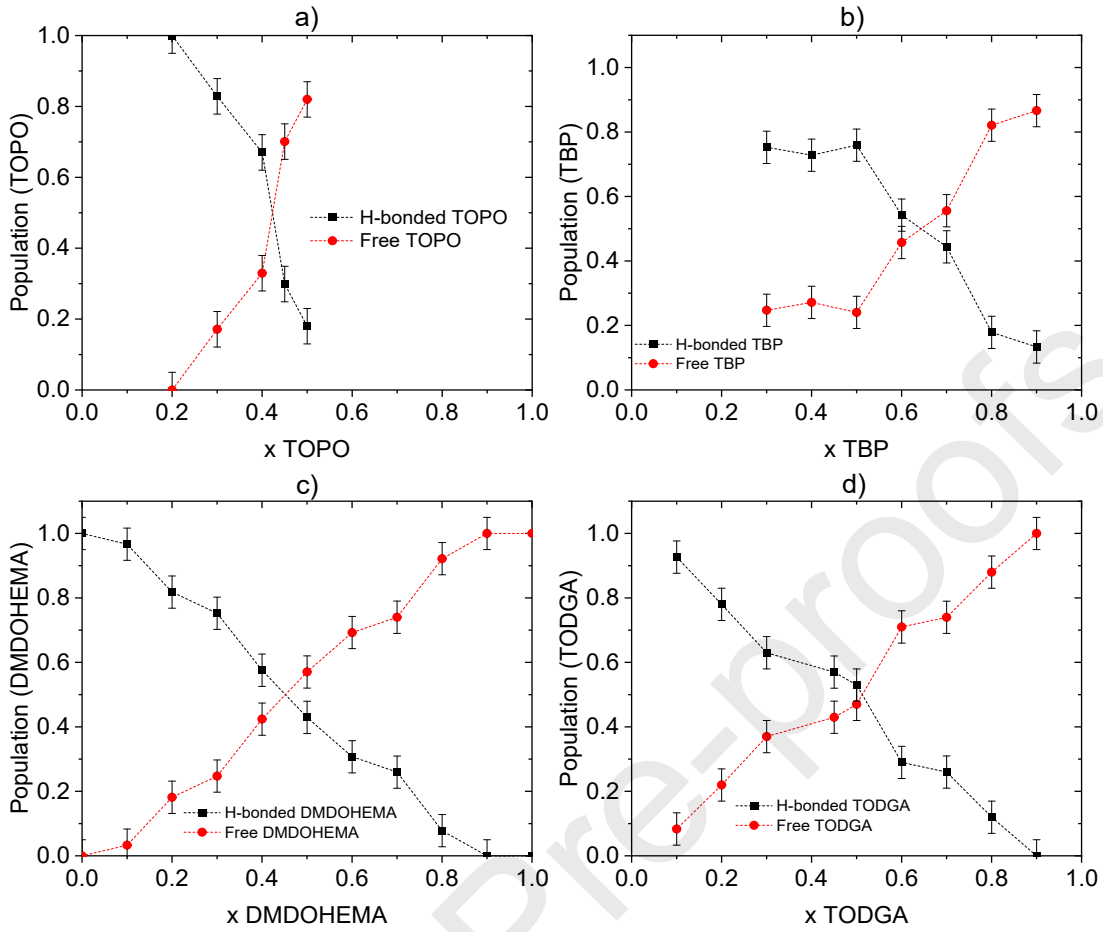

Figure 6: Distribution of hydrogen bonded (black) and free (red) HBA species in the HBA+Decanoic acid eutectic systems as a function of the composition. The relative population was derived from the integration of the FTIR bands presented in Figure 3. Only compositions liquid at room temperature were investigated; octanoic acid instead of decanoic acid was used to determine the population at x_{HBA}=0. Deconvoluted peak areas used in the determination of the H-bonded population is available in **Table S3**.

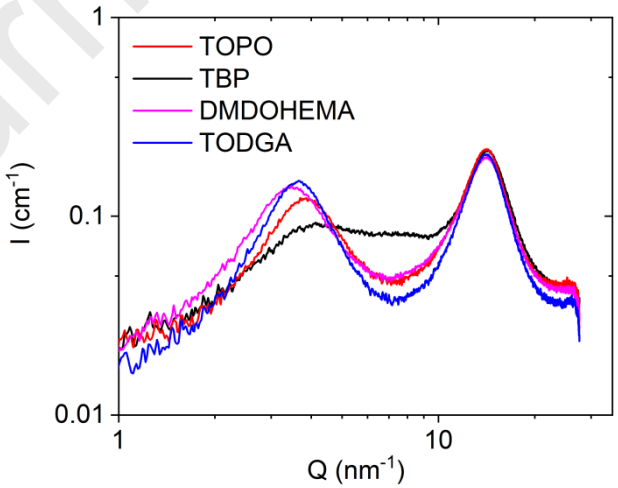

Figure 7: X-rays scattering profile for TBP, TOPO, TODGA or DMDOHEMA with Decanoic acid for a fixed HDES composition of x_{DecAt} = 0.

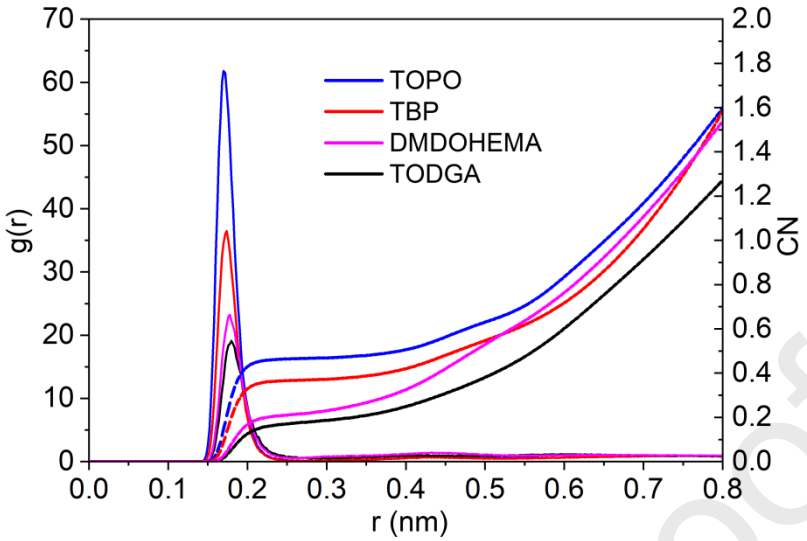

Figure 8: Radial distribution function and coordination number comparison between TOPO,TBP TODGA and DMDOHEMA+ Decanoic acid $x_{extractant} = 0.3$

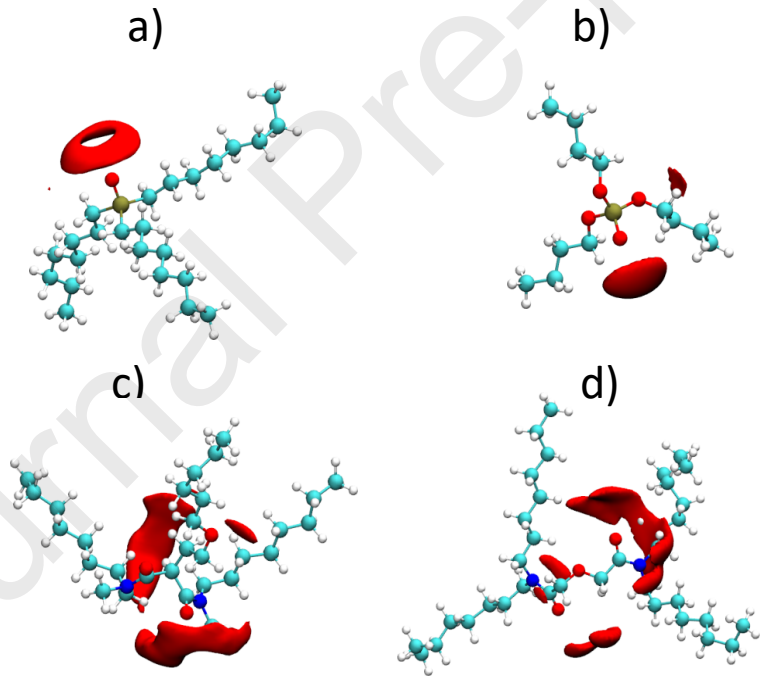

Figure 9: Spatial distribution function of a) TOPO + DecA b) TBP + DecA c) DMDOHEMA + DecA and d) TODGA + DecA, the red area corresponds to the polar head group of Decanoic acid

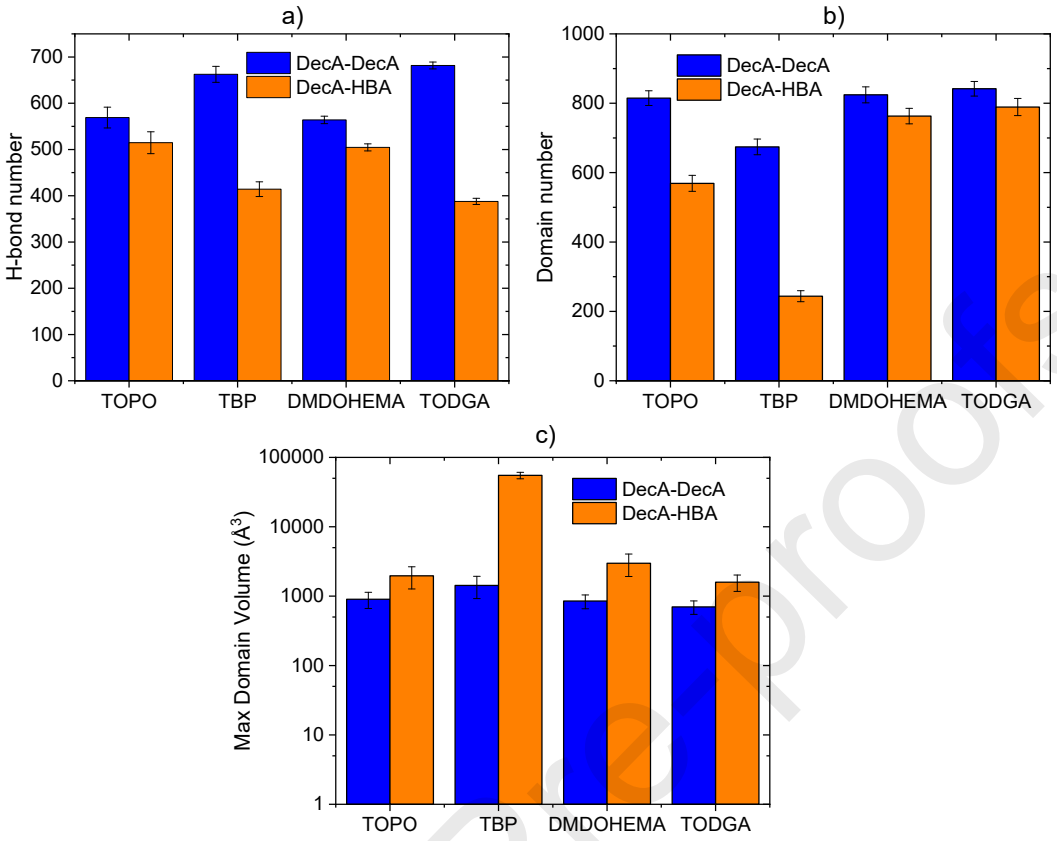

Figure 10: a) H-bond number, b) Domain number, and c) Maximum domain volume comparison between TOPO, TBP TODGA and DMDOHEMA + Decanoic acid for a fixed composition of xDecA = 0.70

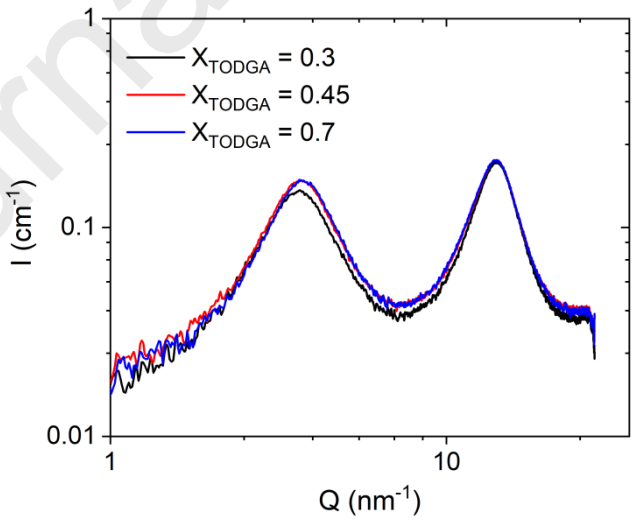

Figure 11: SAXS spectrum of TODGA + Decanoic acid for xTODGA = 0.3; 0.45;0.7

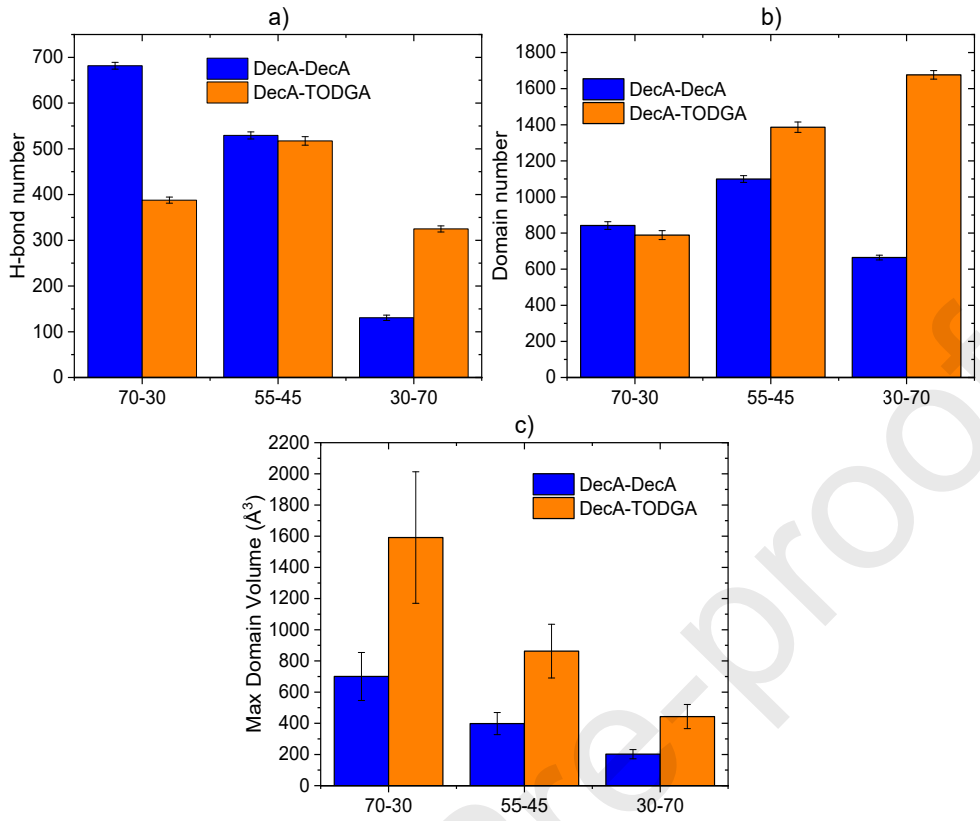

Figure 12: a) H-bond number b) Domain number and c) Maximum domain volume for three ratio of TODGA in TODGA decanoic acid system, in order xTODGA = 0.3;0.45;0.7

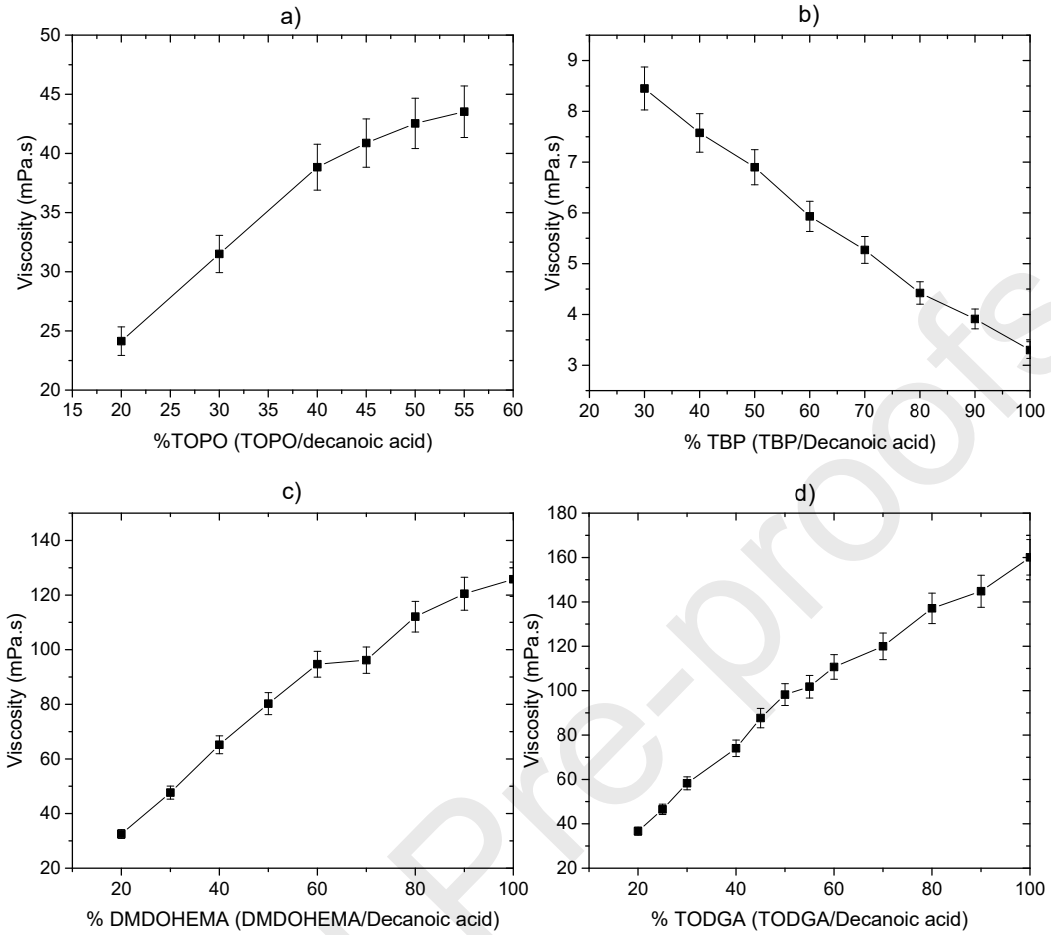

Figure 13: Viscosity of the as-prepared HDES at 25°C for (a) TOPO + Decanoic acid (b) TBP + Decanoic acid (c) DMDOHEMA + Decanoic acid and (d) TODGA + Decanoic acid system as a function of the mixture molar fraction

SI FIGURES

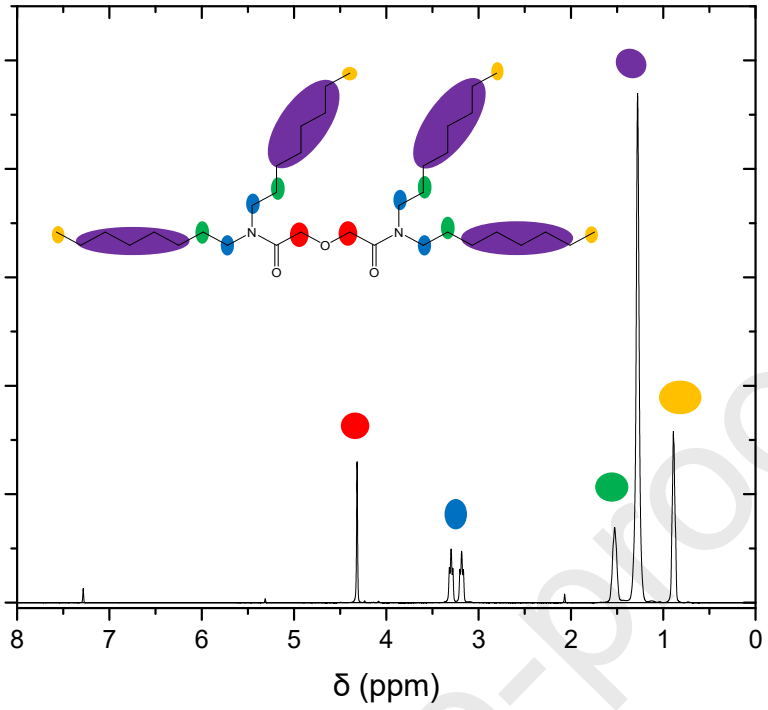

Figure S1: 1H-NMR spectrum of the synthesized TODGA along with the corresponding peak assignments. 1H NMR (400MHz, CDCl3 δ): 4.29-4.34 (4H; -CH2-O), 3.34-3.14 (8H; -CH2-N), 1.59-1.46 (8H; -CH2- CH2-N),1.36-1.20(40H), 0.94-0.84 (12H; -CH3)

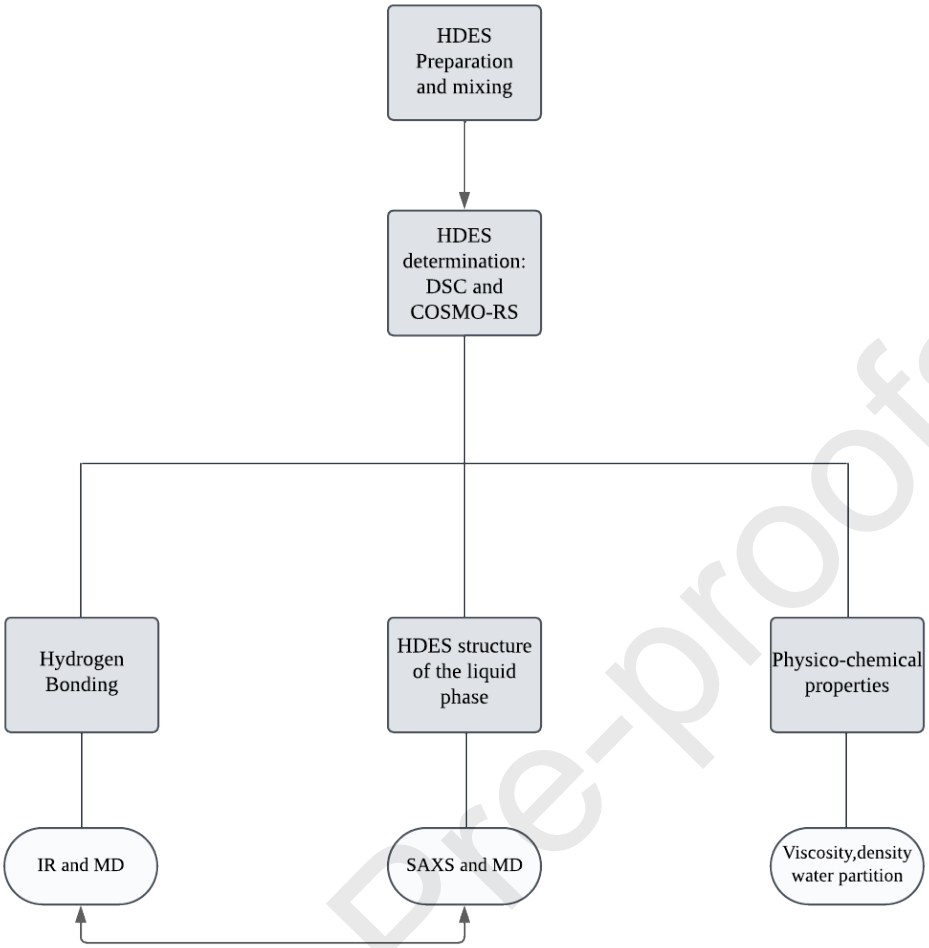

Figure S2: Experimental workflow

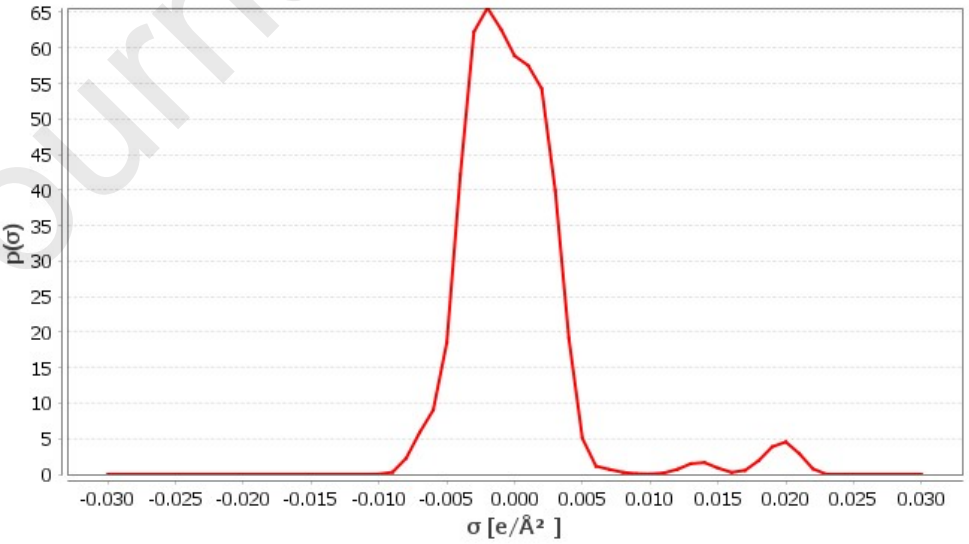

Figure S3: Sigma profile of TOPO based on COSMO-RS optimized structure shown in ***Table S2***.

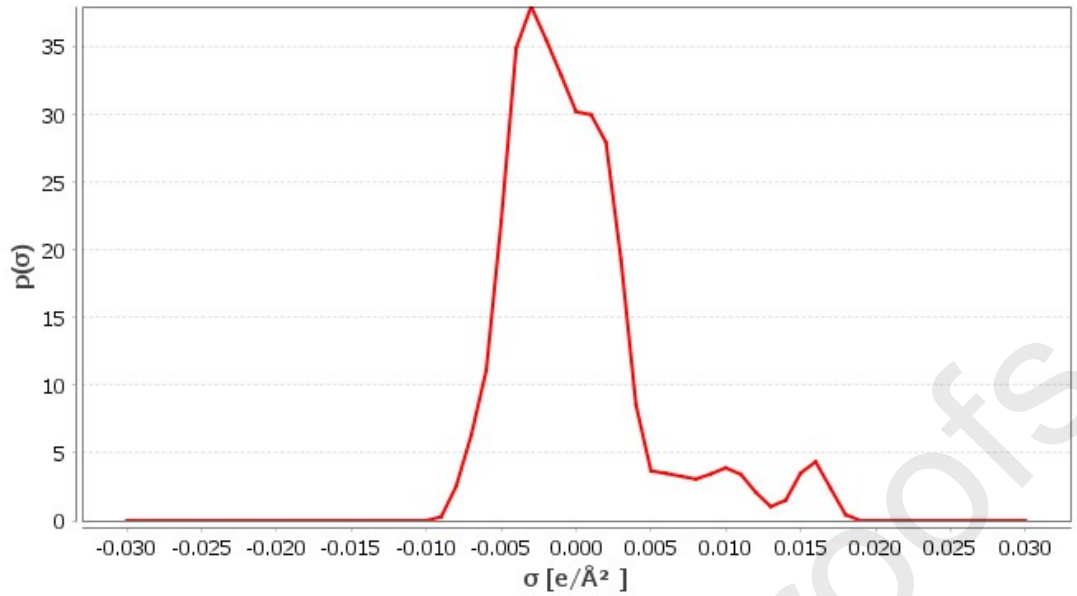

Figure S4: Sigma profile of TBP based on COSMO-RS optimized structure shown in Table S2.

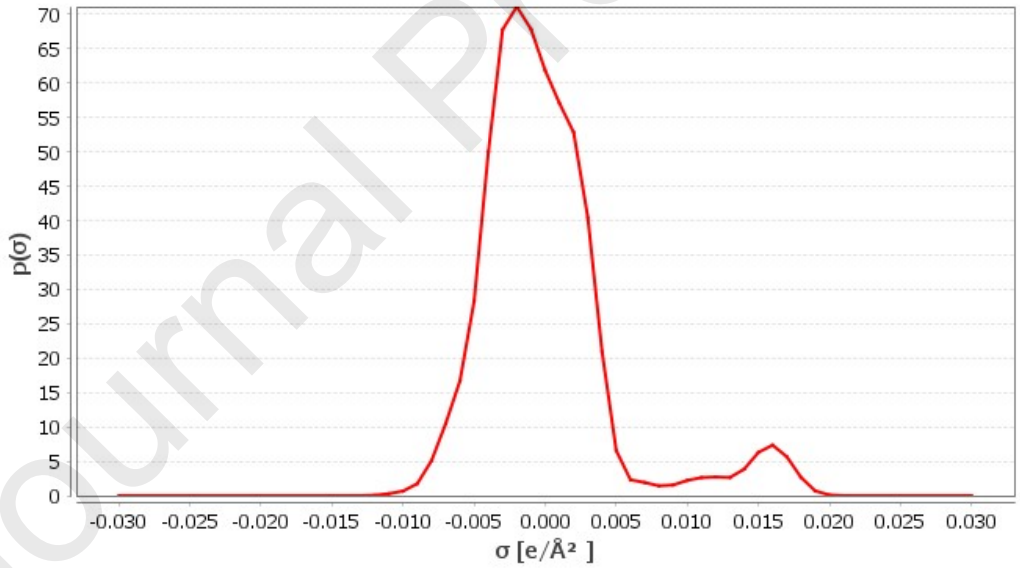

Figure S5: Sigma profile of DMDOHEMA based on COSMO-RS optimized structure shown in Table S2.

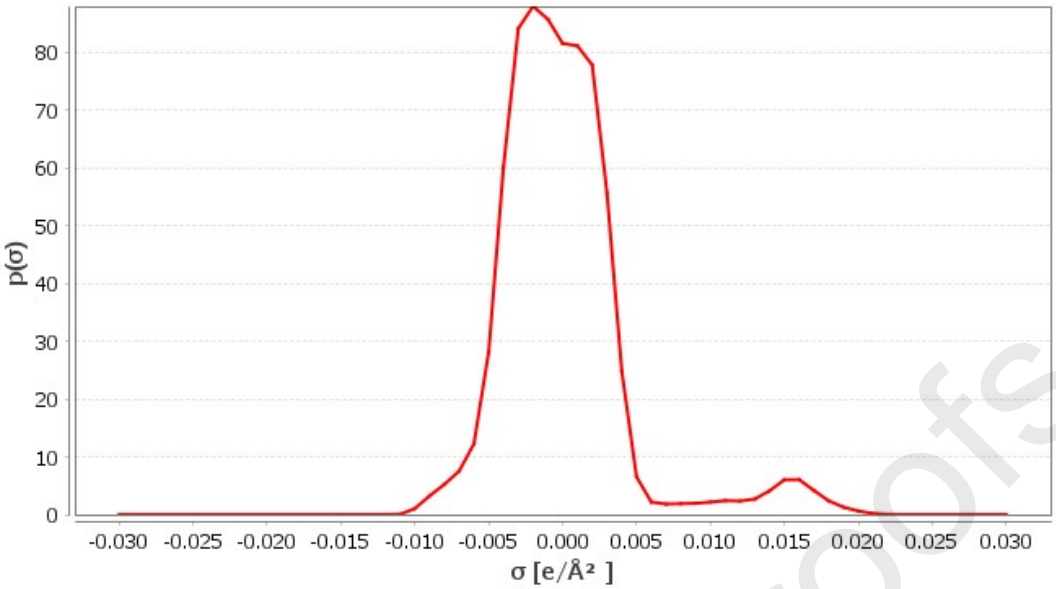

Figure S6: Sigma profile of TODGA based on COSMO-RS optimized structure shown in Table S2.

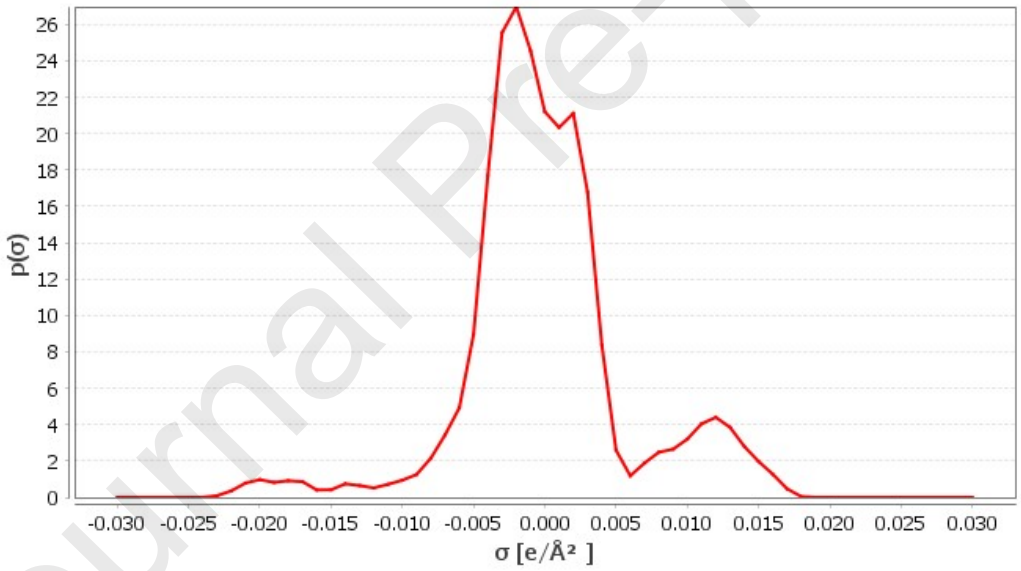

Figure S7: Sigma profile of DecA based on COSMO-RS optimized structure shown in Table S2.

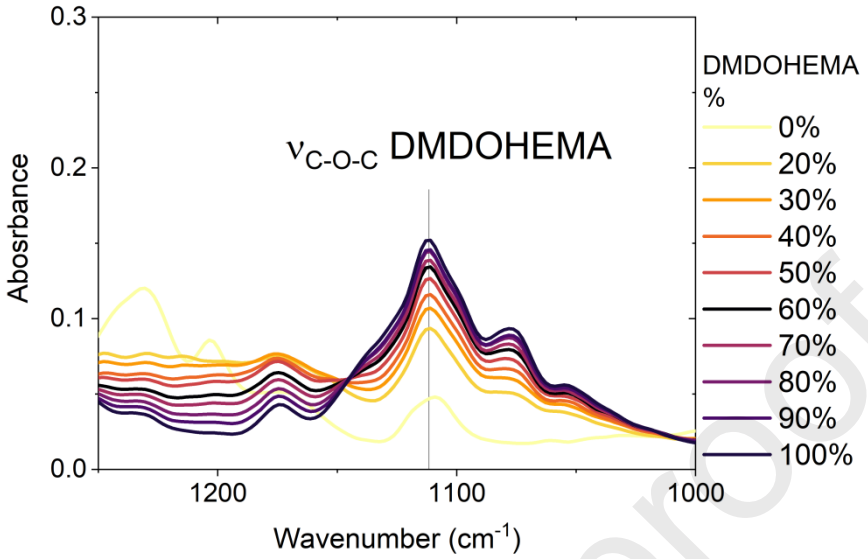

Figure S8: Infrared spectra of DMDOHEMA + DecA as a function of the DMDOHEMA molar fraction focusing on the ether vibration.

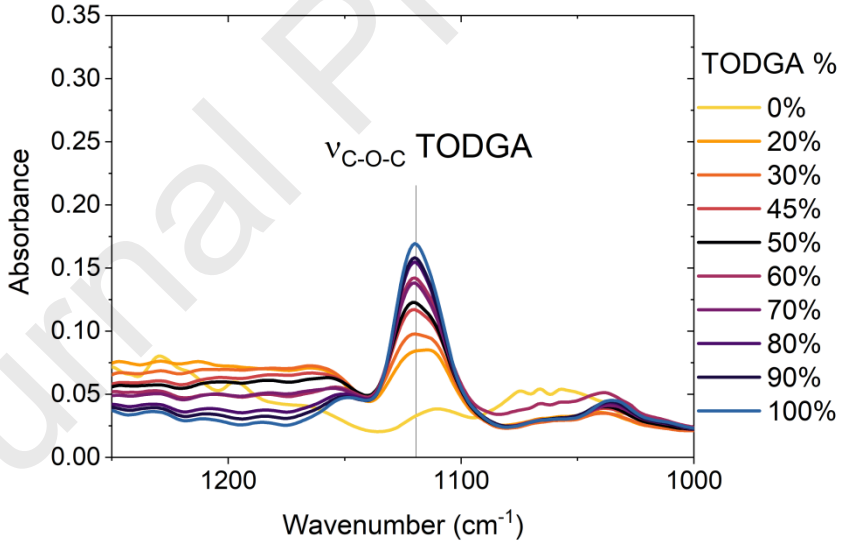

Figure S9: Infrared spectra of TODGA + DecA as a function of the TODGA molar fraction focusing on the ether vibration.

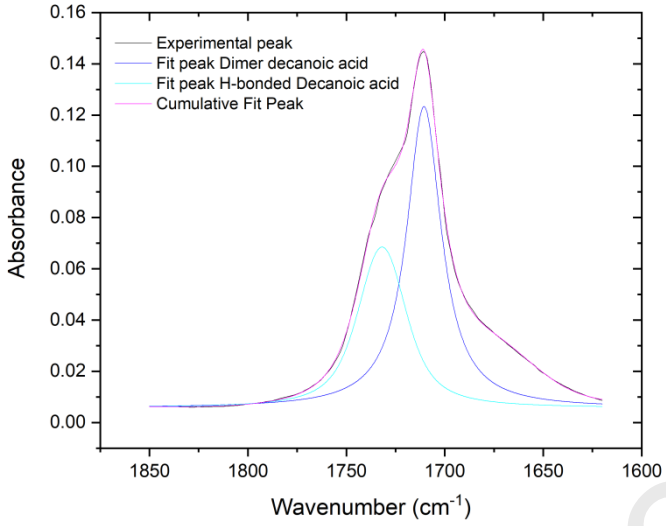

Figure S10: Example of the Gaussian deconvolution procedure followed for the DecA C=O vibration in the TOPO+DecA eutectic system at xTOPO = 0.3.

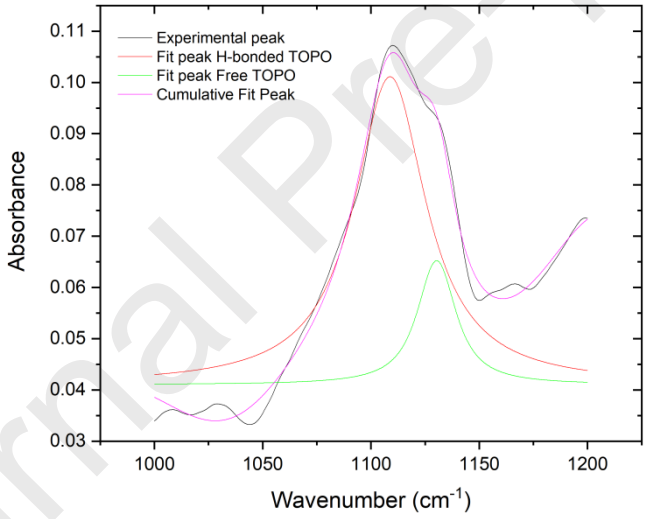

Figure S11: Example of the Gaussian deconvolution procedure followed for the TOPO P=O vibration in the TOPO+DecA eutectic system at xTOPO = 0.3.

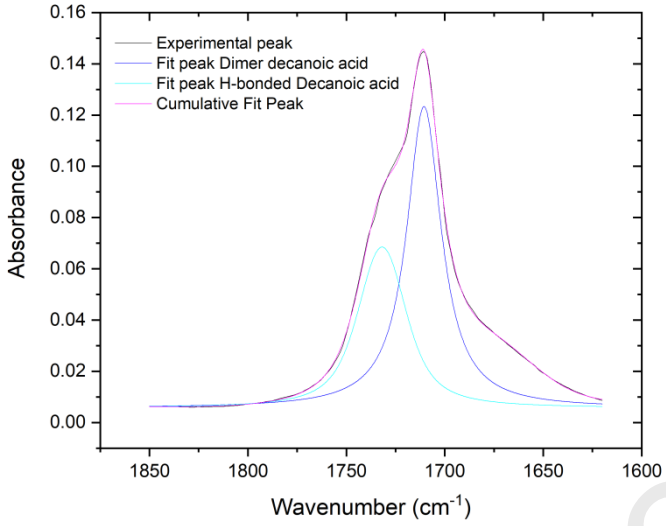

Figure S12: Example of the Gaussian deconvolution procedure followed for the DecA C=O vibration in the TBP+DecA eutectic system at xTBP = 0.3.

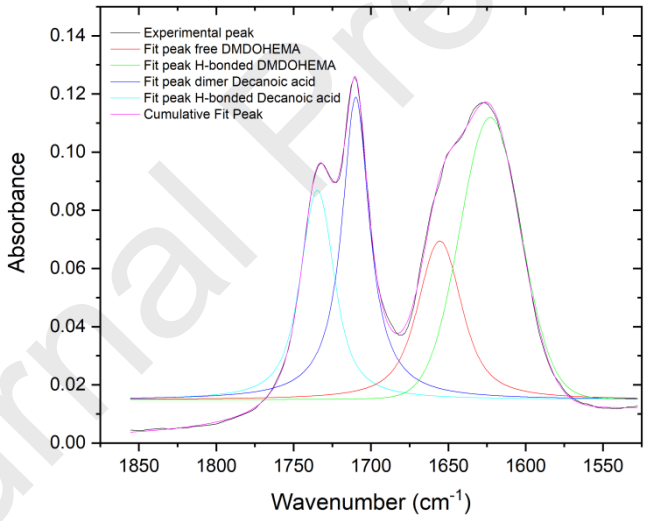

Figure S13: Example of the Gaussian deconvolution procedure followed for the DMODHEMA and DecA C=O vibration in the DMDOHEMA+DecA eutectic system at xDMDOHEMA = 0.3.

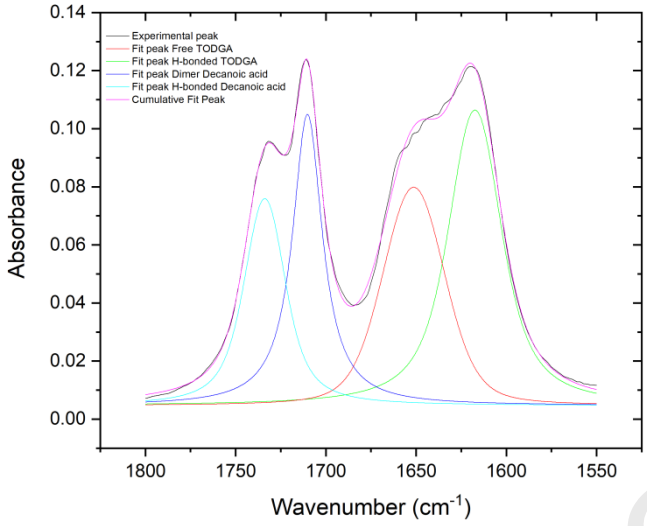

Figure S14: Example of the Gaussian deconvolution procedure followed for the TODGA and DecA C=O vibration in the TODGA+DecA eutectic system at xTODGA = 0.3.

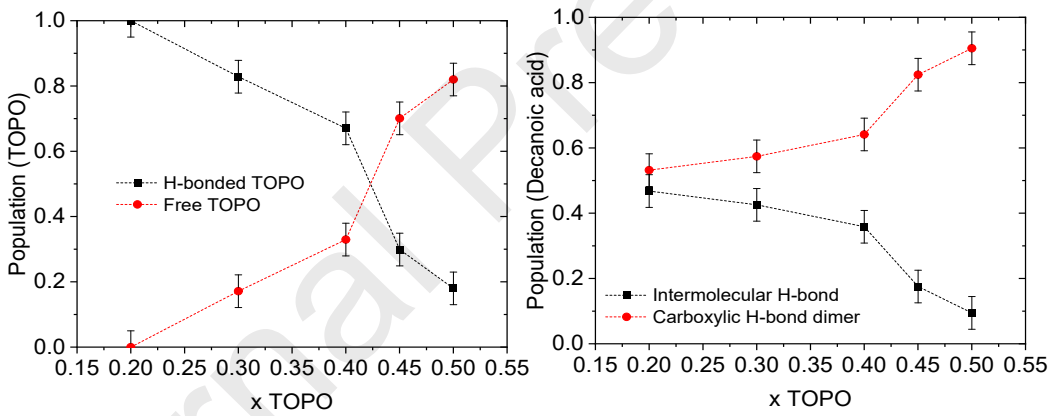

Figure S15: Distribution of hydrogen bonded TOPO (left) and DecA (right) species in the TOPO+DecA eutectic as a function of the composition. The relative population was derived from the integration of the FTIR bands presented in Figure 3a of the manuscript. Only compositions liquid at room temperature were investigated

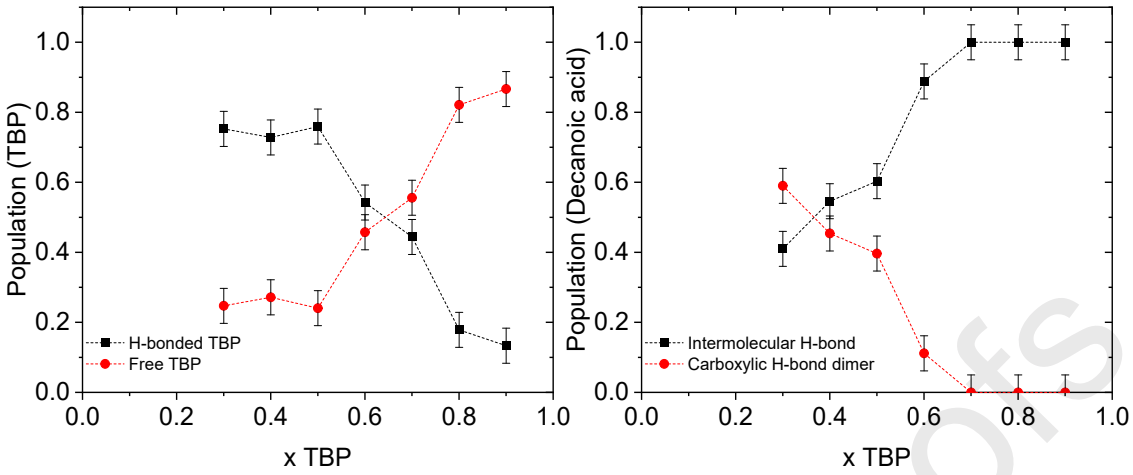

Figure S16: Distribution of hydrogen bonded TBP (left) and DecA (right) species in the TBP+DecA eutectic as a function of the composition. The relative population was derived from the integration of the FTIR bands presented in Figure 3b of the manuscript. Only compositions liquid at room temperature were investigated

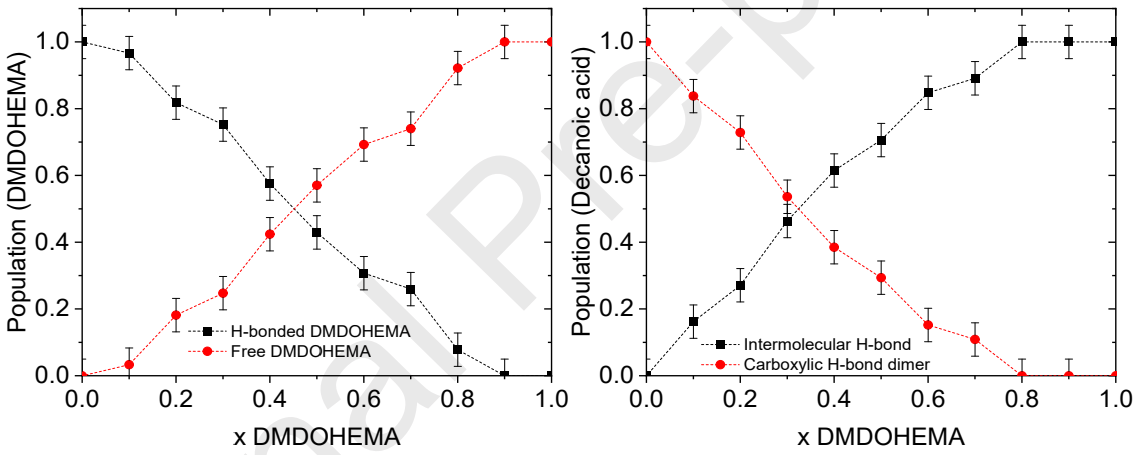

Figure S17: Distribution of hydrogen bonded DMDOHEMA (left) and DecA (right) species in the DMDOHEMA+DecA eutectic as a function of the composition. The relative population was derived from the integration of the FTIR bands presented in Figure 3c of the manuscript. Only compositions liquid at room temperature were investigated. Octanoic acid instead of decanoic acid was used to determine the population at $x_{DMDOHEMA}=0$.

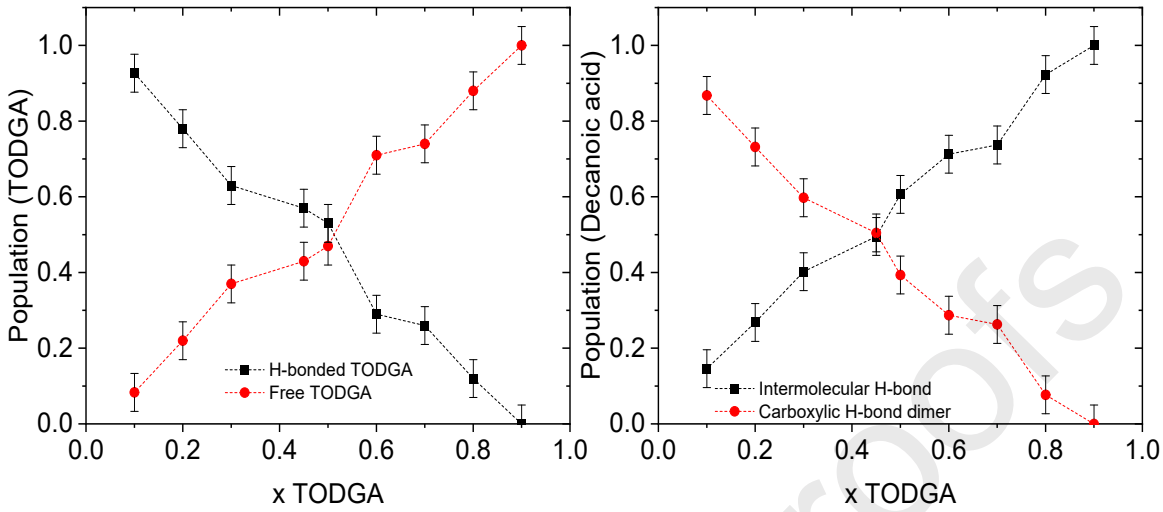

Figure S18: Distribution of hydrogen bonded TODGA (left) and DecA (right) species in the TODGA+DecAeutectic as a function of the composition. The relative population was derived from the integration of the FTIR bands presented in Figure 3d of the manuscript. Only compositions liquid at room temperature were investigated. Octanoic acid instead of decanoic acid was used to determine the population at x_{TODGA}*=0.*

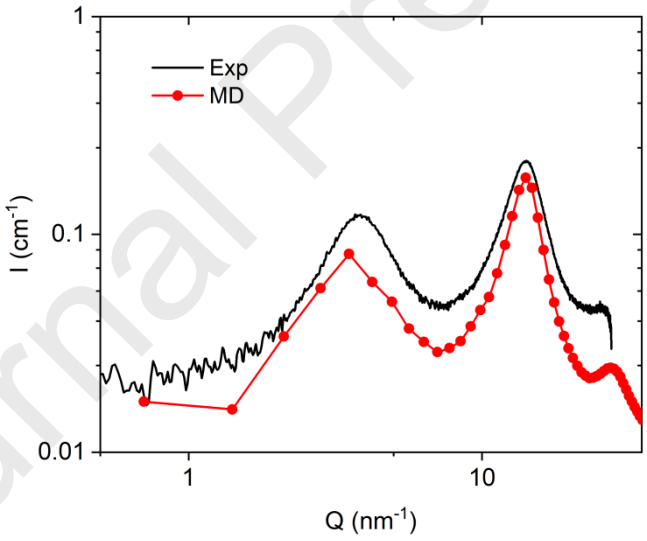

Figure S19: Comparison between the experimental and molecular dynamics SAXS spectra for TOPO+DecA (xDecA = 0.7).

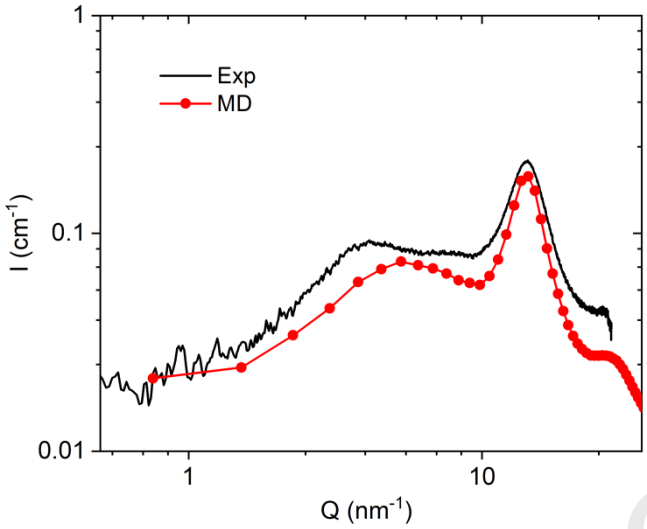

Figure S20: Comparison between the experimental and molecular dynamics SAXS spectra for TBP+DecA (xDecA = 0.7).

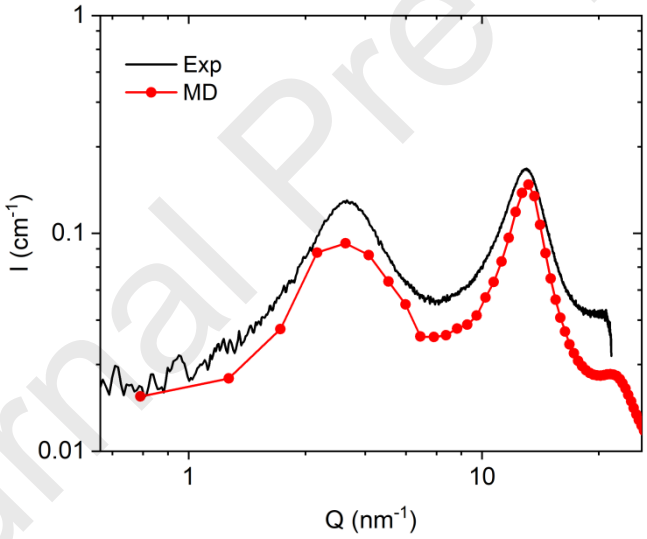

Figure S21: Comparison between the experimental and molecular dynamics SAXS spectra for DMDOHEMA+DecA (xDecA = 0.7)

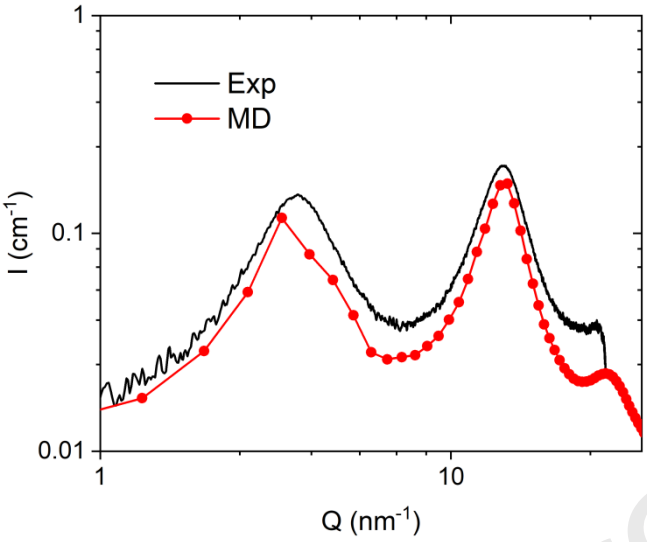

Figure S22: Comparison between the experimental and molecular dynamics SAXS spectra for TODGA+DecA (xDecA = 0.7).

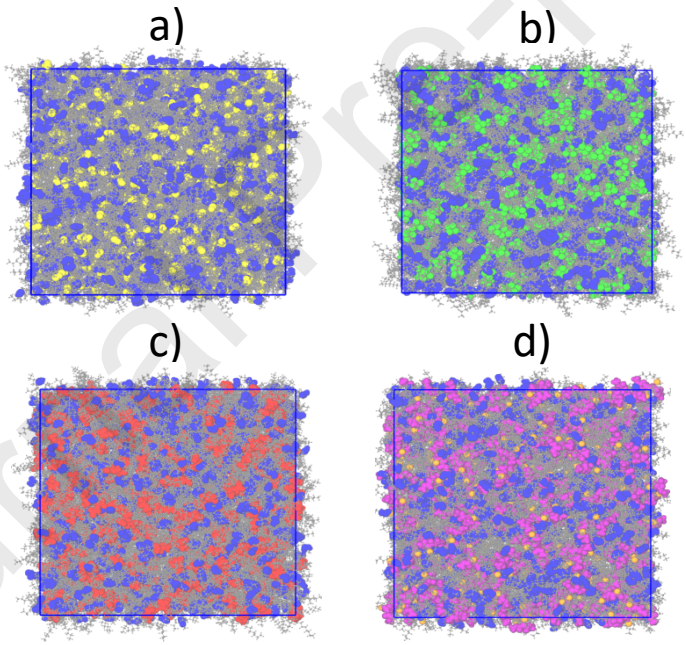

Figure S23: Snapshot of the final equilibration step for the systems composed of a) TOPO, b) TBP, c) TODGA, and d) DMODHEMA with DecA at 298 K for a fixed composition of xDecA=0.7.Color code: yellow – TOPO (P=O), green - TBP (PO4), red - TODGA polar head purple - DMDOHEMA polar head, orange - ether O of DMDOHEMA, grey - alkyl chains.

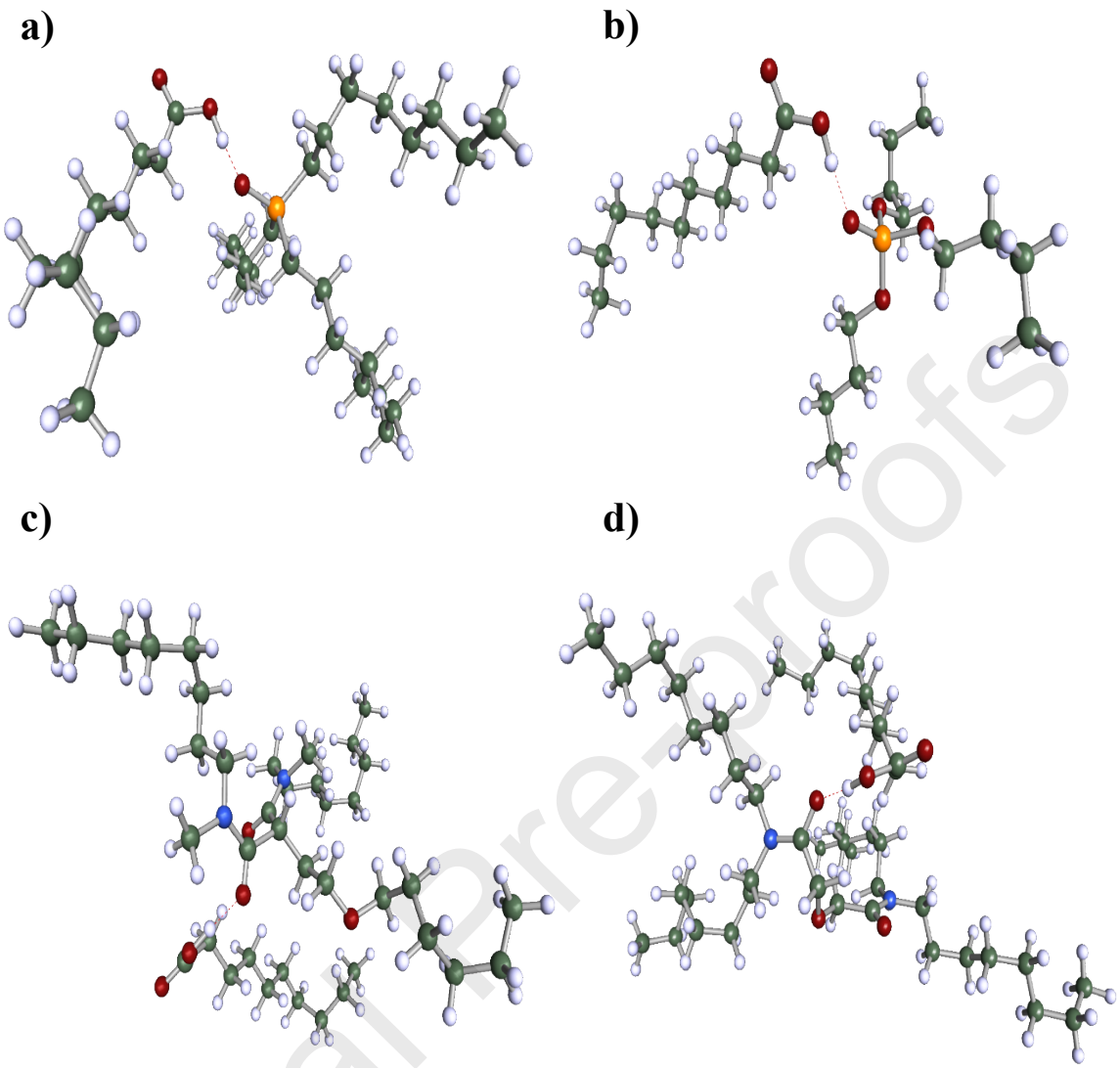

Figure S24: Optimized geometries (COSMO solvation model) of the interaction pairs recognized by COSMO-RS as most probable to occur in the a) TOPO+DecA, b) TBP+DecA, b) DMODHEMA+DecA, and d) TODGA+DecA.

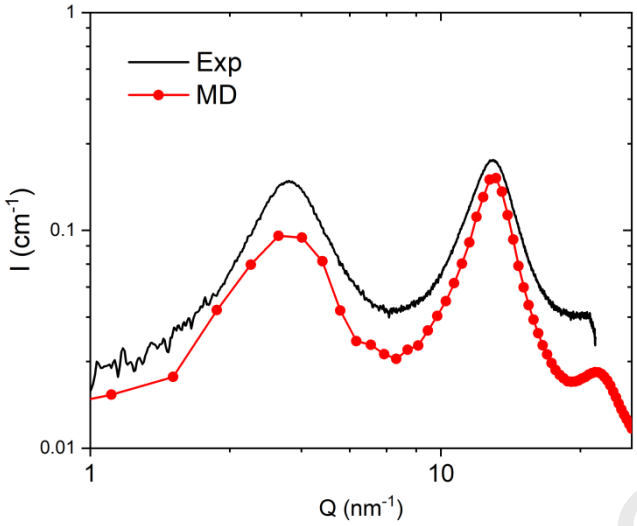

Figure S25: Comparison between the experimental and molecular dynamics SAXS spectra for TODGA+DecA (xDecA = 0.55).

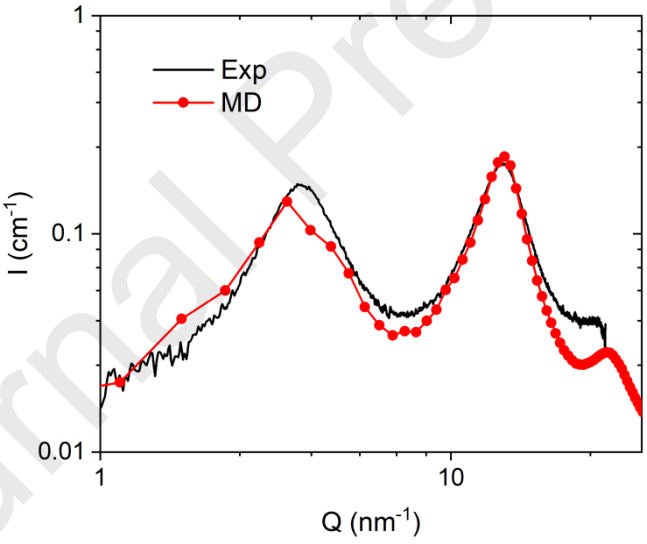

Figure S26: Comparison between the experimental and molecular dynamics SAXS spectra for TODGA+DecA (xDecA = 0.3).

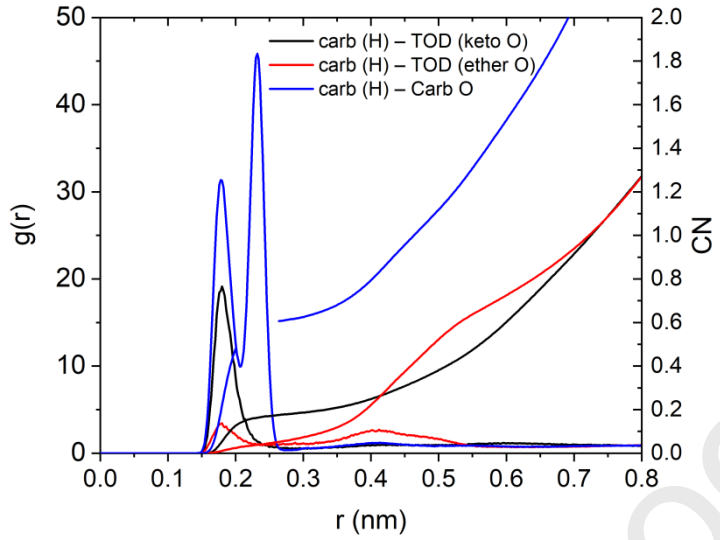

Figure S27: Radial distribution function and coordination number between DecA (carboxylic acid H as reference atom) and TODGA (carbonyl) for a composition of xTODGA= 0.30. The second g(r) peak at 0.24 nm for the DecA– DecA interaction (in blue) corresponds to the intramolecular H-O distance and was corrected in the estimation of the coordination number (CN).

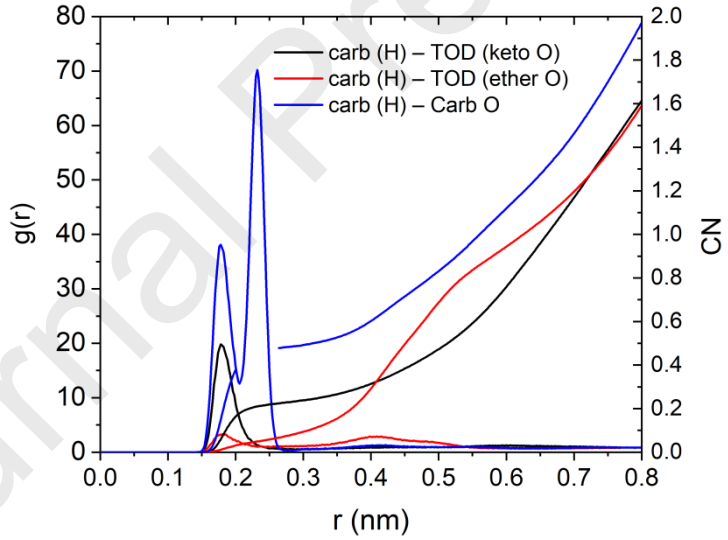

Figure S28: Radial distribution function and coordination number between DecA (carboxylic acid H as reference atom) and TODGA (carbonyl) for a composition of xTODGA= 0.45. The second g(r) peak at 0.24 nm for the DecA– DecA interaction (in blue) corresponds to the intramolecular H-O distance and was corrected in the estimation of the coordination number (CN).

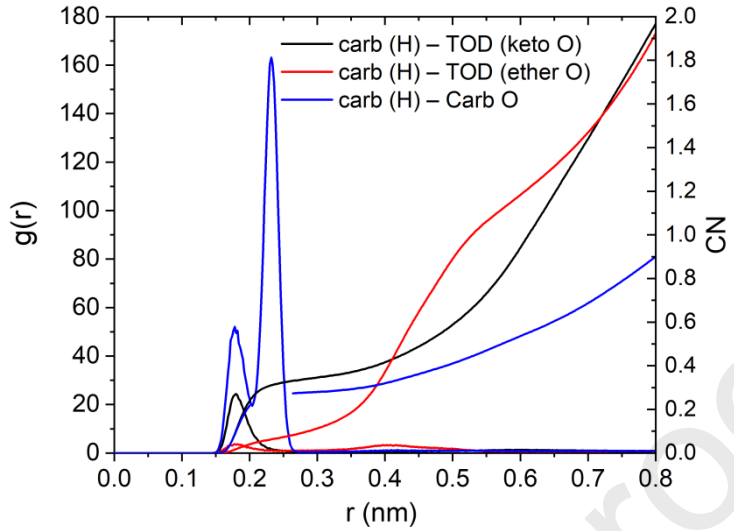

Figure S29: Radial distribution function and coordination number between DecA (carboxylic acid H as reference atom) and TODGA (carbonyl) for a composition of xTODGA= 0.70. The second g(r) peak at 0.24 nm for the DecA – DecA interaction (in blue) corresponds to the intramolecular H-O distance and was corrected in the estimation of the coordination number (CN).